CSIRO

Constraining conceptual groundwater models for the Hutton and Precipice aquifers in the Surat Basin through tracer data

Axel Suckow, Matthias Raiber, Alec Deslandes, Christoph Gerber
February 2018

Citation

Copyright and disclaimer

Important disclaimer

Content

Figures

Acknowledgments

Executive summary

Background

The degree to which Coal Seam Gas (CSG)-driven depressurisation in coal seams is propagated into over- and underlying aquifers and, potentially, surface water features such as wetlands and springs, can only be assessed with thorough understanding of these adjacent aquifers and their degree of connectivity (or lack thereof) with the gas reservoir. The natural water balance for potentially impacted aquifers is often poorly known, but it is important for quantifying the impacts of depressurisation. One of the tools available to assess the water balance of deep aquifers is environmental tracers – substances either dissolved in groundwater or part of the water molecule that provide information about its origin, transport pathways and flow velocity. This GISERA project used new tracer information from several field trips in the Mimosa Syncline and sought to improve the conceptual understanding and to quantify the water balance in the Hutton Sandstone and Precipice Sandstone aquifers, the first and second major aquifers below the Walloon Coal Measures of the Surat Basin, respectively. The Walloon Coal Measures is undergoing development for CSG. The Hutton and Precipice Sandstone aquifers are key regional aquifers supplying farm wells, provide recharge to the Great Artesian Basin and the Precipice Sandstone serves as aquifer for re-injection of CSG water. In this study, groundwater velocity and flow direction in these aquifers were evaluated using environmental tracers.

Current potentiometric surfaces for the Hutton Sandstone have incongruities, such as an apparent groundwater flow towards the hypothesised recharge areas for the aquifer (Hodgkinson *et al.* 2010). Groundwater flow velocity and direction were re-evaluated after sampling some of the regions with poorly constrained conceptualisation as recognized in the earlier study for Gisera W4 (Suckow *et al.* 2016).

The Precipice Sandstone aquifer was unchartered territory concerning environmental tracers prior to the Gisera studies. There are also no recharge estimates known for the deeper part of this aquifer.

- The present study is the first comprehensive multi-environmental tracer study in the Precipice Sandstone and allows an estimate of flow velocity and recharge to the deeper Precipice Sandstone.
- Flow velocities and recharge values in the Precipice Sandstone are higher than in the Hutton Sandstone and significant in comparison to the Gubberamunda Sandstone. The groundwater flow system in the Precipice Sandstone continues south of the Dawson River.
- Earlier findings for the Hutton Sandstone are confirmed: it is characterised by a double porosity system and flow takes part in only a small part of the formation. Effective recharge to the deeper Hutton is much smaller than earlier estimates. Flow is restricted to the north of the Dawson River, further south waters are beyond the dating range of $^{36}Cl/Cl$.

However, the Precipice Sandstone increasingly serves as water supply aquifer for the local cattle industry and is also used for re-injection of CSG production water. A multi-tracer study was planned and conducted here to understand the flow system in the Precipice Sandstone, quantify flow velocities from the recharge areas into the deep aquifer and to derive an estimate of recharge.

The tracers considered and sampled for included major ions, tritium (^3H), stable isotopes of the water molecule ($^{18}O/^2H$), ^{14}C, ^{36}Cl, noble gases, and $^{87}Sr/^{86}Sr$. The radioactive tracers ^{36}Cl and ^{14}C were interpreted in more detail because these can estimate groundwater flow velocities at a suitable scale for the aquifers in question (>10,000 years). Tracer distribution along transects from the recharge areas to depth were interpreted using several conceptualizations of the geochemical and hydrogeological environment, such as the input of 'dead' Cl from neighbouring aquitards, dead carbon from oxidation of organic carbon and a single versus double porosity aquifer. This allowed to confirm the earlier findings in (Suckow *et al.* 2016) for the Hutton Sandstone and a first conceptualization of the groundwater flow system in the Precipice Sandstone as well as a first quantification of flow velocities and recharge rates.

Key results

PRECIPICE SANDSTONE

This study allowed the first quantification of flow velocities in the Precipice Sandstone using environmental tracers. Groundwater in the Precipice Sandstone is much fresher than in the Hutton Sandstone and moves much faster. We found no indication that the Precipice is a double porosity system such as the Hutton Sandstone. Flow velocities derived from ^{14}C are in the range of 0.8 m/y to 1.5 m/y and there is no observable decrease of the ^{36}Cl/Cl ratio with radioactive decay. The noble gas and stable isotope data confirm the findings from radiocarbon. The flow system of the Precipice Sandstone seems not to be restricted to the Dawson River as discharge area but continues towards the south. This raises the question as to which aquifer the water of the Precipice contributes to, because this formation is only found in Queensland and seems to end at depth (Ransley *et al.* 2015). A first estimate of deep recharge into the Precipice Sandstone was possible from these findings and is quantified to 110 mm/y to 315 mm/y. Together with the vertical cross-sectional area within the Mimosa Syncline this corresponds to a total recharge of 1.1 GL/y to 6.6 GL/y.

HUTTON SANDSTONE

Most of the earlier findings about the Hutton Sandstone in (Suckow *et al.* 2016) were confirmed by the new analyses. The Hutton Sandstone is a double porosity system, distance velocities are in the range of 1m/y but flow happens only in 50m or less compared to the total formation thickness of 250m. There is a difference between flow directions inferred from environmental tracer results and potentiometric heads (Hodgkinson *et al.* 2010). The potentiometric head surface is most probably a more recent development, caused by anthropogenic influence or climate change while the tracer results display a view on the flow system that corresponds to the natural pre-development state (several thousand years).

The stable isotope record interpreted as palaeoclimate record in (Suckow *et al.* 2016) is not in agreement with the findings in the Precipice Sandstone, in which no climate-related shift to more negative values in ^{18}O and ^{2}H was observed. Since these negative values of ^{18}O and ^{2}H are correlated with ^{14}C and ^{36}Cl/Cl at the detection limit, the waters can be of any age larger than the dating range, which due to the double porosity in this case is around 30 ky. New noble gas and helium concentration measurements also confirm these findings.

Conclusion and recommendations

The differences in the inferred groundwater flow direction in the Hutton Sandstone between the contemporary potentiometric surface and environmental tracers suggest that this system may be in a transition phase. The contemporary piezometric surface may reflect ongoing changes driven by climate or extraction whilst tracers would reflect the natural flow system prior to development. The trends in the environmental tracers support the concept of the low effective transmissivity of the Hutton and much smaller recharge than previously assumed, making this system more vulnerable to groundwater extraction or to depressurisation in neighbouring geological formations than anticipated. In other words, as only a small proportion of the aquifer effectively transmits water, the sustainable yield for this aquifer is probably low. Determining the connectivity of the Walloon Coal Measures to the Hutton Sandstone should still be considered a key knowledge gap, particularly in the central part of the Mimosa Syncline where previous work suggested that the hydrochemistry of these two units shows strong similarities (Raiber and Suckow 2017).

The study identified several key knowledge gaps, including:

1. The magnitude of groundwater flow in the Hutton Sandstone from the south-eastern recharge area towards the centre of the Mimosa Syncline and the extent of connectivity between the Clarence-Moreton Basin and the Surat Basin is not known

2. The water balance for the Hutton Sandstone remains poorly defined since it probably disintegrates into smaller flow systems between the branches contributing to the Dawson River. This complicates the assessment of the potential impacts of depressurisation in the Walloon Coal Measures or of groundwater extraction from this aquifer.

3. It remains unclear whether the groundwater in the Hutton Sandstone south of the main branch of the Dawson River is a stagnant water body or if and where it is recharged from. Such an assessment would need tracers operating on longer time scales than used here (>1My) and since the available tracers are dissolved gases ($^{40}Ar/^{36}Ar$, ^{21}Ne, ^{136}Xe) they would also need specialized sampling approaches (Banks *et al.* 2017).

Key recommendations from the study include:

1. Use the tracer distribution in the Hutton Sandstone and Precipice Sandstone as additional calibration target for improving numerical groundwater flow and solute transport modelling

2. Continue efforts to quantify the connectivity between the Walloon Coal Measures and neighbouring geological formations.

Recommendation 1 will be targeted by modelling efforts within this project.

1 Introduction

The degree to which Coal Seam Gas (CSG)-driven depressurisation in coal seams is propagated into adjacent aquifers and, potentially, surface water features such as wetlands and springs will depend to a large degree on how well adjacent aquifers are connected or disconnected from coal seams. Measuring this connectivity is not a simple task because of the complexity of coal-bearing subsurface environments, including the presence of multiple aquifers and aquitards, faults and fractures. Even when a connection exists, quantifying impacts can be difficult because the water balance for most deep aquifers is poorly known. Only if this water balance and detailed baseline knowledge on geochemical and environmental tracer concentrations is established, can CSG impact be detected as changes from this baseline. Two previous GISERA projects evaluated the connectivity (Smith 2015) and the water balance (Suckow *et al.* 2016) for key geological formations of the Surat Basin. In this report, we build on one of the previous projects by re-evaluating groundwater flow direction and velocity in the Hutton Sandstone, the first major aquifer below the Walloon Coal Measures of the Surat Basin. For the first time this study also undertook a detailed tracer study in the Precipice Sandstone, underlying the Hutton and a target aquifer for re-injection of treated CSG water. The Walloon Coal Measures is undergoing development for CSG, whilst the Hutton and Precipice Sandstone aquifers are key regional aquifers used for farm water supply and a component of the Great Artesian Basin (GAB), a nationally significant hydrogeological system (Smerdon et al. 2012).

The assessment of the water balance for the Hutton Sandstone and Precipice Sandstone aquifers was largely made using environmental tracers – natural or anthropogenic trace substances in groundwater that provide clues as to its origin and movement. The tracers considered included major ions, stable isotopes of the water molecule ($^{18}O/^{2}H$), ^{14}C, ^{36}Cl, noble gases and tritium (^{3}H). However, ^{36}Cl, ^{14}C and noble gases were analysed in more detail because these can quantify groundwater flow velocity at a suitable scale (>1000 years). Existing environmental tracer data from the earlier GISERA Baseline project (Suckow *et al.* 2016) was incorporated in the analysis and the data was supplemented by (i) targeted sampling of 24 wells during a CSIRO-led field trip, (ii) an additional seven samples taken by the companies (Origin Energy, QGC and Santos), and (iii) ten samples taken during two field trips in cooperation with the Office of Groundwater Impact Assessment (OGIA). The sampling area extended from the recharge areas in the north to deeper sections of the aquifer further south, with the southmost samples taken just south of Miles.

- This study focused on the Precipice Sandstone and used environmental tracers to derive groundwater flow velocities and a recharge value for this aquifer.
- Additional samples were taken in the Hutton Sandstone to close knowledge gaps.

In the following, a review of the hydrogeological environment is provided. The historical and new tracer data collected were interpreted to evaluate both groundwater flow direction and velocity in the Hutton and Precipice. The interpretation of environmental tracers to evaluate groundwater flow processes can be quite complex (IAEA 2013; Suckow 2014) and is covered in several scientific text books. Since it cannot be reviewed in detail here, the interested reader is provided with a very short summary on environmental tracers and the processes important for this report in Appendix A following page 34.

2 Methods

2.1 Study area

The Surat Basin is a 440,000 km² intracratonic basin of south-central Queensland and north-central New South Wales. It consists of up to 2,500 m of layered sediments of Jurassic-Cretaceous age. The Surat Basin overlies the Permo-Triassic Bowen Basin, which extends farther to the north up to the latitude of Rockhampton (-23.4°N, see inset in Figure 2.4 where the blue area is the Bowen Basin), whereas the northern margin of the Surat Basin is defined by the northern outcrop of the Jurassic formations (Precipice Sandstone at the latitude of Bundaberg, -24°N). Both basins were formed by sedimentation of a trough extending from north to south, the Mimosa Syncline. Changes in the sedimentary environment over time resulted in the formation of several aquifers, intercalated aquitards and coal bearing formations in the Surat and the Bowen basins. Key hydrostratigraphical units in the Mimosa Syncline include (from top to bottom, see also Figure 2.1): the Mooga Sandstone (aquifer), Orallo Formation (aquitard), Gubberamunda Sandstone (aquifer), Walloon Coal Measures (coal bearing formation, containing aquifer & aquitard layers), Hutton Sandstone (aquifer), Evergreen Formation (aquitard) and the Precipice Sandstone (aquifer) (Hodgkinson *et al.* 2010). The underlying Moolayember Formation (aquitard) and Clematis Sandstone (aquifer) are part of the Bowen Basin.

- The study area can be described as a layered cake of aquifer-aquitard systems in a natural depression.
- New groundwater samples were obtained in the Precipice and Hutton for 41 wells and combined with existing data.
- To ensure robust analysis necessary in old groundwater systems, a multi-tracer approach was adopted to obtain multiple lines of evidence for interpretation.
- Simple zero- and one-dimensional models were used to check data for consistency and to describe the governing factors of groundwater flow

The Surat Basin is regarded as part of the Great Artesian Basin (GAB). The western margin of both the Surat and the Bowen Basin is defined by the Nebine Ridge, where the aquifers of the Surat and Bowen basins thin out but are assumed to be connected to the aquifers of the Eromanga Basin of the GAB further to the west (Habermehl 1980; Radke *et al.* 2000). The eastern margin of Surat and Bowen basins is defined by the Kumbarilla Ridge, where both are connected to the Clarence Moreton Basin. In the south, the Surat Basin extends far into New South Wales and includes the Coonamble Embayment and the Oxley Basin, both overlying the Gunnedah Basin (Habermehl 1980). The deepest formation in the Surat Basin is the Late Triassic-Early Jurassic Precipice Sandstone, which unconformably overlies the Triassic formations of the Bowen Basin (Figure 2.1). The Precipice Sandstone is isolated from the overlying Hutton Sandstone by a shale-rich horizon at the top of the formation and by the Evergreen Formation aquitard (Hodgkinson *et al.* 2010). The Walloon Coal Measures have variable hydraulic properties. Whereas the upper and lower parts of the Walloon Coal Measures form aquitards, the hydraulic transmissivity of the inner section is significantly larger (Esteban *et al.* 2015). Further to the south and centre of the Mimosa Syncline, the Walloon Coal Measures are overlain by the Springbok Sandstone, which is considered an aquifer and equivalent to the Adori Sandstone in other parts of the GAB. It is overlain by the Westbourne Formation (aquitard), Gubberamunda Sandstone (aquifer) Orallo Formation (aquitard) and Mooga Sandstone aquifer (Hodgkinson *et al.* 2010). The Mooga and Gubberamunda Sandstones together are considered equivalent to the Cadna-owie Hooray Aquifer of the Eromanga Basin (Radke *et al.* 2000; Smerdon and Ransley 2012). Two structural faults exist at the margins of the Mimosa Syncline, which created only minor deformations and displacements in the Jurassic-Cretaceous sequence. Both run north-south and are reactivated Permo-Triassic fault systems. They are described as the Hutton-Wallumbilla fault in the west and the Moonie-Goondiwindi and Burunga-Leichhardt fault system in the east (hereafter referred to as the Burunga-Leichhardt fault).

The best quality groundwater in the Mimosa Syncline is found in the Gubberamunda Sandstone and Precipice Sandstone aquifers. However, the Gubberamunda Sandstone can only be found south of Wandoan (see Figure 2.4 and all following maps) and the Precipice Sandstone can only be assessed at

greater depth. Water from the Hutton Sandstone generally has a higher salinity and the formation has a lower yield. Extensive sediment core testing for hydraulic conductivity by the enterprises engaged in CSG exploration (mainly lab triaxial permeability) generally gave a wide range of values for the Hutton Sandstone of roughly six orders of magnitude of $(1 \cdot 10^{-5}-1)$ m/day in both vertical and horizontal direction. Values for the Precipice were generally higher and less variable (0.001–10) m/day; (APLNG 2014). There are also lateral differences in the hydrochemistry of groundwater, with generally fresher water in the Hutton Sandstone close to the northern and western outcrops and much higher salinities towards the south and east, especially east of the Burunga-Leichhardt fault and south of Wandoan (APLNG 2014).

2.1.1 RECHARGE AREAS

The sedimentation history into the basement trough and the later erosion of the sediment layers explains the shape of the outcrop areas, which resembles an upside-down 'U' around Taroom and Injune for the Hutton Sandstone and Precipice Sandstone (see Figure 2.4 and all following maps). The later deposited Springbok, Gubberamunda Sandstone and Mooga Sandstones, which outcrop north of the Roma-Wallumbilla-Miles line but south of the Injune-Wandoan line, show this 'U' shape to a much lesser extent. In this report the outcrop areas are functionally all regarded as recharge areas for the respective aquifers and the terms 'outcrop area' and 'recharge area' are used interchangeably.
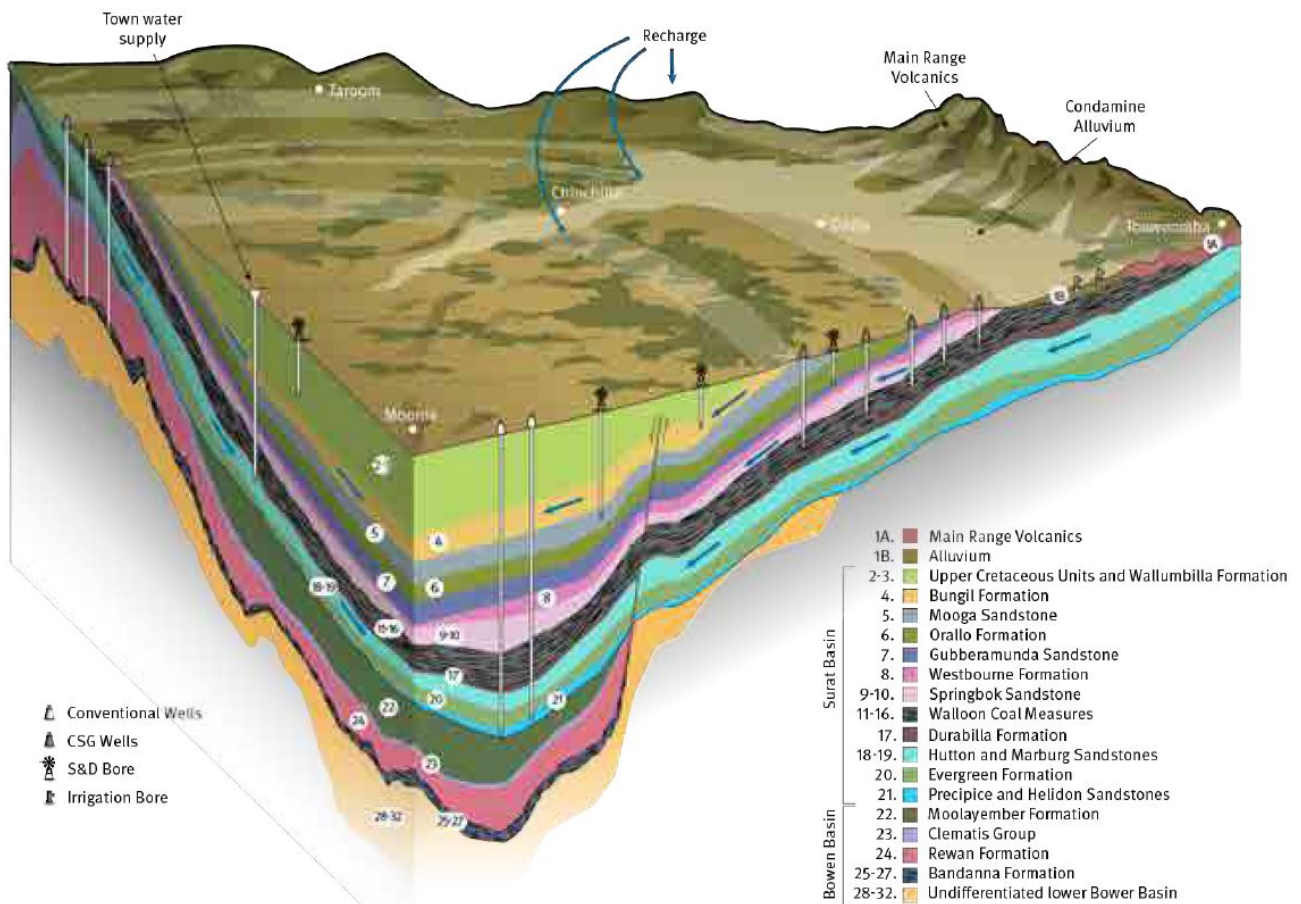
Figure 2.1: Conceptual model of the groundwater systems in the Surat Cumulative Management Area (OGIA 2016)

2.1.2 POTENTIOMETRIC SURFACE IN THE HUTTON AND PRECIPICE SANDSTONE AQUIFERS

The potentiometric surface for the Hutton and Precipice Sandstone was recently evaluated by Hodgkinson et al. (2010) (Figure 2.2). Major recharge areas would occur to the north and east and the inferred

groundwater flow would fan in several directions from there, including to the south, north-east and east. Groundwater flow to the north-east appears focussed around Dawson River tributaries (Figure 2.3).
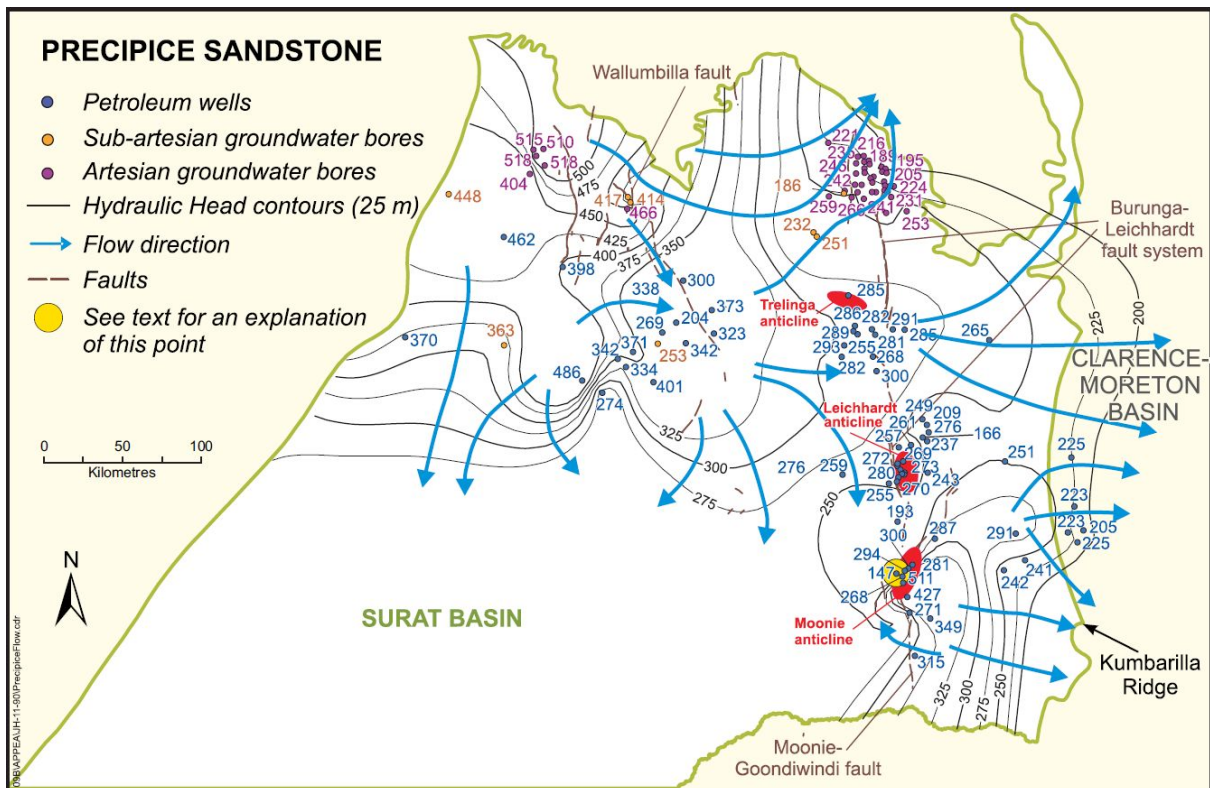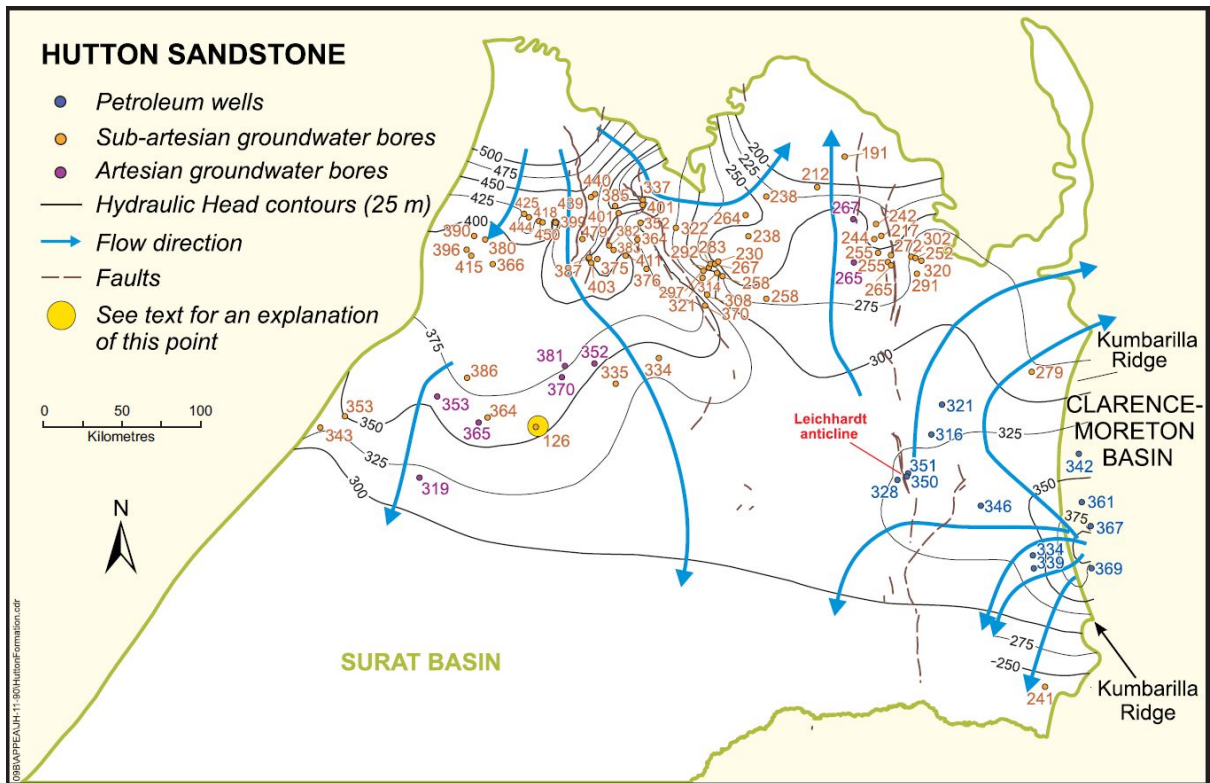
Figure 2.2: Potentiometric surface for the Hutton and Precipice Sandstone inferred by geophysical methods (Hodgkinson et al. 2010)
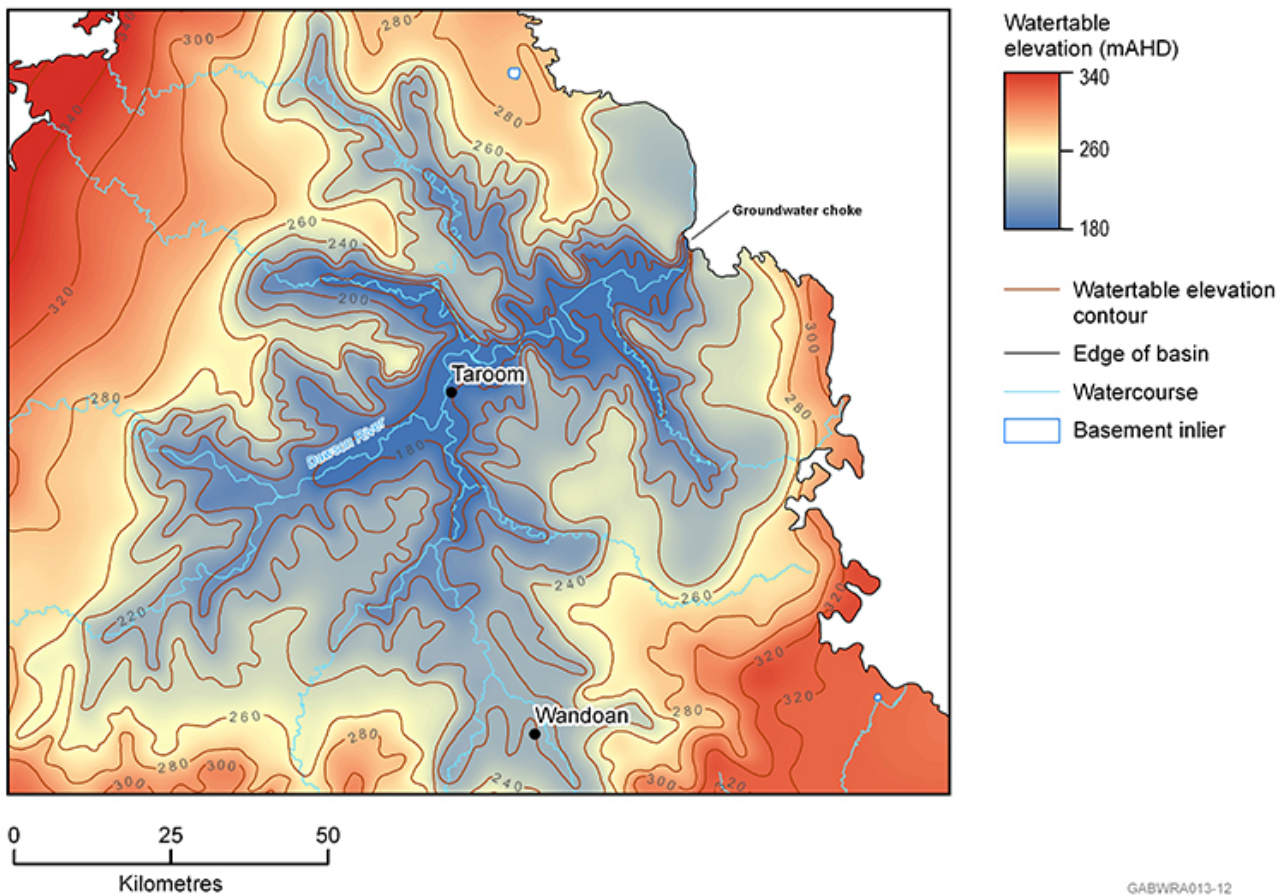
Figure 2.3: Potentiometric surface for the Hutton Sandstone in the vicinity of the Dawson River catchment inferred using geophysical techniques (Ransley and Smerdon 2012)

At the Mimosa Syncline, the Hutton outcrops towards Taroom and, further south, towards Wallumbilla. Using water level measurements in bores (corrected for salinity and temperature), the potentiometric surface for the Hutton Sandstone shows a depression centred around Taroom. This implies groundwater is flowing towards the outcrop, which is counterintuitive. Hodgkinson *et al.* (2010) found similar results for the Evergreen Formation and Precipice Sandstone.

2.2   Experimental design for the field study

Using environmental tracers, a field study was designed to determine whether or not groundwater flow is principally from north to south in the Mimosa Syncline, as the potentiometric surface indicates. In a first step, the available environmental tracer database for the Hutton Sandstone was reviewed. Two databases were combined, one from Geoscience Australia ('GA database'; Feitz *et al.* 2014) and another from the GABWRA project ('GABWRA database'; Ransley and Smerdon 2012). In general, ^{14}C and ^{36}Cl was higher in recharge areas, consistent with a north to south flow direction (that is, the concentration for both tracers will tend to decrease in a downstream direction because of radioactive decay). These findings were used in the first GISERA project (Suckow *et al.* 2016) to identify wells along two transects in the Mimosa Syncline and focussing on the Hutton Sandstone. The wells selected for this first field study aimed to best fill the gap in space for ^{14}C and ^{36}Cl measurements and thus provided a more rigorous evaluation of groundwater flow direction and velocity for this section of the Hutton Sandstone. As a result, the Hutton Sandstone was described as a double porosity system in which groundwater flows only in a small part of the total thickness (Suckow *et al.* 2016).

The first study revealed several knowledge gaps that needed to be addressed to better understand details of the Hutton Sandstone groundwater flow system and to derive a first quantitative understanding of groundwater flow and its time scales in the Precipice Sandstone aquifer. Identification of appropriate

groundwater bores for environmental tracer sampling was again conducted using the Queensland Digital Groundwater Database (QDGWD) provided by the State Of Queensland (DNRM 2013). The two overarching requirements for identifying a bore as appropriate were: 1) the aquifer/hydrostratigraphic formation the bore was open or screened to was well known and could be tested by the available hydrochemical data 2) the geographic location of a given bore in relation to the recharge areas, as well as being situated as equally spaced as possible towards the Reedy Creek and Condabri industrial sites. In addition, information relating to the operational status of the facility (such as recent hydraulic head data) and the presence or absence of on-ground or down-hole equipment (such as headworks or windmills) was considered to ensure a bore was practical for sampling. Once a suitable spatial distribution and a practical number of bores were identified and plotted, property information specific to each bore was used to acquire contact details of landholders and industry representatives. Through contact with landholders and industry, basic information specific to individual bores sites were confirmed and the provision of site access was established in a verbal and written format. This resulted in the sampling locations shown in Figure 2.4.

Despite the anticipated relatively old age for groundwater along the transects (>10,000 years) both 'young' (^{3}H) and 'old' (^{14}C, ^{36}Cl and ^{4}He) groundwater tracers were sampled in order to evaluate potential mixing between young and old groundwater sources, as recommended in text books for dating old groundwater (IAEA 2013). The presence of 'young' tracers could either reflect a natural or artificial (i.e. bore leakage) connectivity with a shallower aquifer. This needs to be assessed, and if necessary corrected for, before using a tracer like ^{14}C and ^{36}Cl to derive flow velocities. Major ions, noble gases and δ^{18}O/δ^2H of water were also measured to either help calibrate other tracers (i.e. Cl for ^{36}Cl/Cl dating) or provide an additional dating tool in the form of an anticipated palaeoclimate signal (δ^{18}O/δ^2H). Additional bores were sampled in the Precipice and Gubberamunda sandstones (usually in the vicinity of bores sampled in the Hutton Sandstone) to collect vertical tracer profiles across key hydrostratigraphical units.
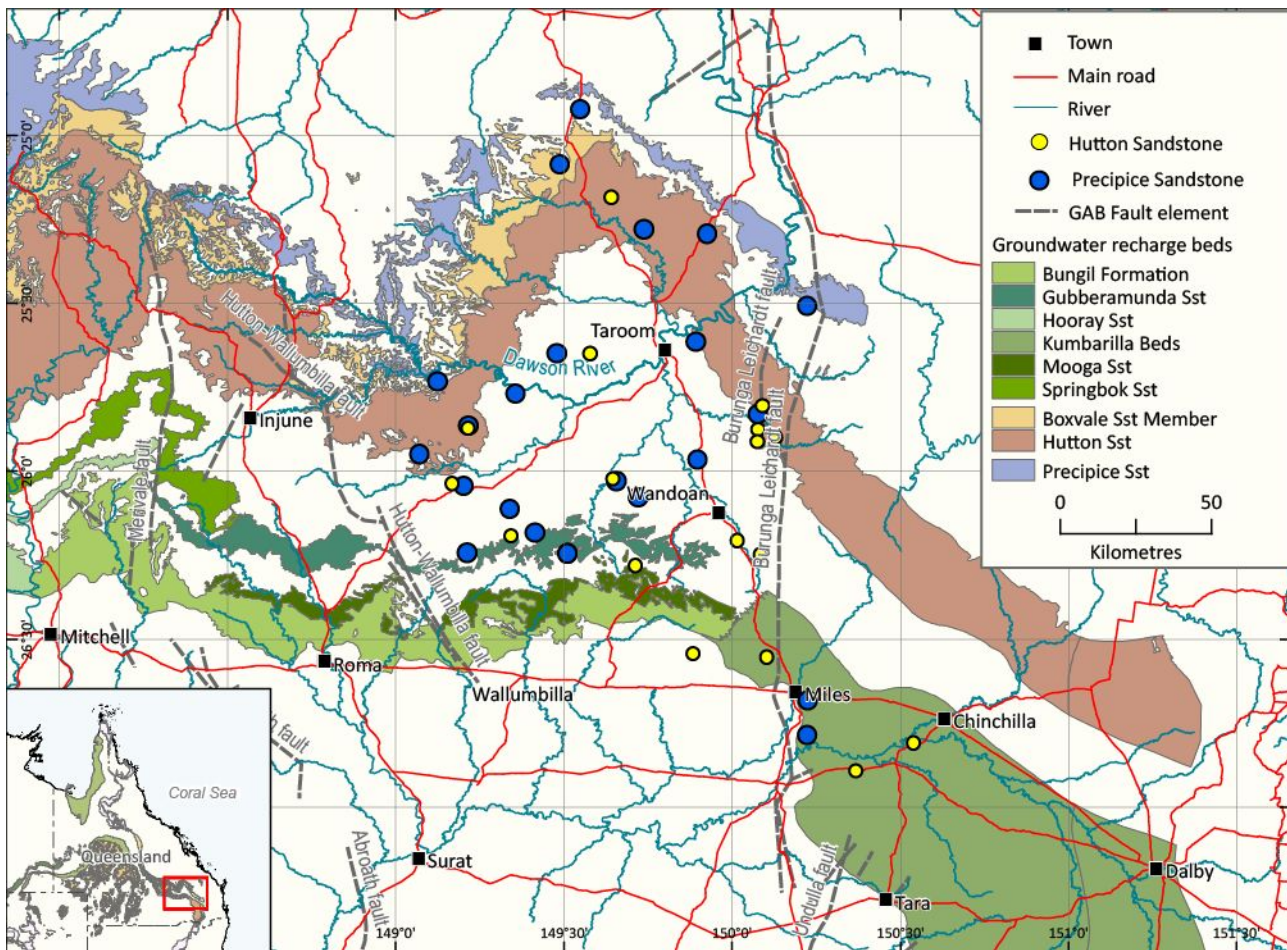
Figure 2.4: Position of the new sampling locations in Hutton Sandstone and Precipice Sandstone.

Samples were obtained during an extended field trip by CSIRO in March-April 2017. This sampling trip was complemented by additional samples taken by Santos and QGC (no noble gas samples) and by a cooperation with OGIA (Peter Khor & Steve Flook) who obtained bore samples during their several field trips investigating groundwater-surface water connections.

2.3   Field sampling methods

2.3.1   PURGING OF BORES

At each bore, groundwater was carefully purged to ensure representative water samples from the aquifer were obtained. Purging at a given bore was conducted using existing infrastructure, which varied from headworks on artesian bores, to Mono pumps, Grundfos submersible pumps and Airwell Pumps on sub-artesian bores. Hydraulic head and bore construction data obtained from the QDGWD was used to calculate the total purge volume at each site, usually three standing water columns. On occasions, some bore sites needed less purging due to recent pumping or natural artesian flow. Conversely, some bore sites required additional purging volumes until monitored chemical parameters (electrical conductivity (EC), pH and temperature) stabilised.

2.3.2   FIELD PARAMETERS

Chemical parameters were monitored and recorded during purging and sampling under gently flowing conditions, including EC, pH and temperature. Electrical conductivity, pH and temperature were monitored

using a handheld submersible TPS WP-81 water quality meter. The presence of H_2S was noted qualitatively when detected (odour) during sampling as was the amount of gas bubbles.

2.3.3   SAMPLE COLLECTION

Sampling for all tracers was conducted by initially establishing a gas-tight connection to existing headworks (on artesian bores) and discharge hose (on sub-artesian bores). In the case of artesian bores, a gas-tight connection was established by securing copper or nylon tubing using Swagelok fittings directly to the headworks. For sub-artesian bores, copper or nylon tubing was secured to agricultural pipe using Philmac adaptors. These gas-tight connections are most important to prevent sample contamination with the atmosphere.

Groundwater samples were collected for laboratory analysis of general chemistry (pH, EC and alkalinity) as well as major and minor ions. Duplicate samples for major and minor ions were collected, filtered with a 0.45 µm Acrodisc syringe filter and placed in 125 mL PET plastic bottles. Samples for cation analysis were acidified with nitric acid (HNO_3). For δ^2H and $\delta^{18}O$, duplicate samples were collected, filtered with a 0.45 µm syringe filter, and placed in a 28 mL gas-tight glass bottle (McCartney bottle) to prevent evaporation. Strontium isotope samples were collected in 500 mL PET bottles. Tritium samples were collected in 1 L PET plastic bottles under gently flowing conditions to avoid excessive air contact and capped without a head space to avoid contact with the atmosphere. Duplicate or triplicate samples for dissolved noble gases were collected in copper tubes following Weiss (1968). Briefly, this involved creating a gas tight connection between the copper tube and the discharge outlet on the bore, gently flushing the tube, and applying a back pressure using a flow regulator before clamping the copper tube at each end without trapping any gas bubbles. However, for the deepest bores pumping hot water (>60°C), degassing of sampled water was not always avoidable. In these cases, a fractionation of noble gas values cannot be excluded, although samples were taken such that gas bubbles were not enclosed within the copper tubes. This was achieved by turning the copper tube upside down after closing the first clamp and letting the gas bubbles escape to the connecting tubing.

Samples for tritium (^3H), ^{14}C and ^{36}Cl were collected in 1 L PET plastic bottles filled to the top and capped tightly without any head space.

2.4   Analytical methods

Major and minor ion concentrations were determined at CSIRO Analytical Services Unit (ASU) Waite Campus Adelaide. Cations were analysed by inductively coupled plasma optical emission spectrometry (ICP-OES) and anions by ion chromatography. Samples for δ^2H, $\delta^{18}O$ and $\delta^{13}C$ were analysed at the University of Queensland where measurements were made using an Isoprime mass spectrometer following, for δ^2H, reduction at 1100°C using a Eurovector Chrome HD elemental analyser and for $\delta^{18}O$, by water equilibration at 25°C using an Aquaprep device. Strontium isotope ratios ($^{87}Sr/^{86}Sr$) of all groundwater samples were analysed at the University of Melbourne using multi collector-inductively coupled plasma mass spectrometry (MC-ICP-MS).

Samples for ^{14}C analysis were measured by accelerator mass spectrometry (AMS) at the Australian Nuclear Science and Technology Organization (ANSTO), Lucas Heights. Samples were prepared by first precipitating the dissolved inorganic carbon from 1 L of groundwater as strontium carbonate ($SrCO_3$) under alkaline conditions (pH >11). The $SrCO_3$ precipitate was then acidified and purified cryogenically into aliquots of carbon dioxide (CO_2) for measurement by AMS. Samples for ^{36}Cl were also measured via AMS at ANSTO, Lucas Heights. Prior to measurement samples were prepared as pure silver chloride (AgCl). Samples for tritium were analysed at the tritium laboratory of ANSTO, Lucas Heights by electrolytic enrichment and subsequent liquid scintillation counting.

Noble gas concentrations (He, Ne, Ar, Kr, Xe) were determined at the CSIRO Environmental Tracer Laboratory (ETL), Waite Campus, Adelaide. Measurement involves 1) separation of all dissolved gases from water using an off-line high vacuum extraction system; 2) separation of all reactive gases from noble gases

by several getter systems; 3) separating the noble gases from each other using cryo techniques and 4) measuring the noble gas fractions with quadrupole mass spectrometry. All noble gas concentrations are given in cubic centimetre of gas per gram (cc(STP)/g where STP stands for Standard Temperature and Pressure and the gram are related to the weight of the sample, not to fresh water).

2.5 Lumped Parameter Models

A single scalar 'age' (e.g. '30 years-old') is not appropriate to describe a groundwater sample because, due to dispersion and mixing, groundwater samples contain water recharged at different times, represented as an age distribution. This holds especially true in aquifers with very long timescales of groundwater flow (greater than several thousand years) because mixing, dispersion and diffusion of tracers become more important for longer times. It is also not necessary to determine groundwater 'age' from tracers because many hydrogeological processes can be inferred from tracer concentrations alone. Therefore, no attempt is made here to deduce any 'apparent ages' (Suckow 2014), as this was regarded as not appropriate. Instead, binary tracer-tracer plots, tracer depth profiles and tracer transect profiles were interpreted using zero-dimensional lumped parameter models (LPMs), one-dimensional flow interpretation or other simple approaches. Lumped parameter models are simplified representations of aquifers and flow systems that can be used to understand what are the key hydrogeological processes (advection, dispersion, mixing, etc.) impacting on tracer distribution (see (Suckow 2014) and A.1 for additional discussion on the concept of groundwater age).

The lumped parameter models used here were the Piston flow Model (PM), the Exponential Model (EM) and the Binary Mixing Model (BMM). The PM assumes that no mixing takes place and that all water particles within the sample represent the same age. This corresponds to the conventional (human) understanding of the word age (Suckow 2014) and also to the particle tracking approach in discretised numerical flow models (Pollock 1994). The EM assumes an exponential age distribution in the samples. Mathematically this is equivalent to the flow system in an extremely simplified aquifer with homogeneous recharge, homogeneous transmissivity and porosity and constant depth, sampled using a well screened over the whole aquifer (Vogel 1967). It is also mathematically consistent with a well-mixed system (e.g. a lake) with constant inflow and outflow. As a special property, the youngest water always has the largest relative contribution in an Exponential Model. The BMM assumes that the sample consists of exactly two water sources with a widely differing age – one assumed to be very young and the other very old (that is, free of any anthropogenic or radioactive tracers in question). The interested reader is referred to specialised literature (Maloszewski and Zuber 1985; Cook and Böhlke 1999; Solomon *et al.* 2006; Suckow 2013) for more detailed information on LPMs and mean residence times. All data handling and lumped parameter model calculations were performed with the LabData database and laboratory management system (Suckow and Dumke 2001) which includes 'Lumpy', a package for lumped parameter models (Suckow 2012).

To further evaluate the effect of geochemistry (such as dead ^{14}C and ^{36}Cl inputs from aquitards) or of the flow system (single versus double porosity aquifer) on tracer distribution, additional simple models were used. These included the Phillips (IAEA 2013) ^{36}Cl model and the Sudicky and Frind (1981) model for diffusion-dominated tracer transport. These are described in more detail in A.1.

3   Results

Combining the historical and the new information collected during this study, a significant environmental tracer database was established for the Hutton Sandstone and the Precipice Sandstone aquifers in the Mimosa Syncline. As usual and necessary the data were evaluated in a stepwise manner: results will be first presented as a general assessment of the isotope patterns and then by individual aquifer. This analysis also enabled evaluation of some of the parameters required for further interpretation of the data, such as the likely initial ^{14}C and ^{36}Cl concentrations entering the aquifer (which are required to evaluate groundwater velocity). Relevant tracers

- Tracers for young groundwater (decades) were at the detection limit, indicating that the Precipice and Hutton contain no groundwater younger than 50 years.
- Lack of young groundwater indicates the sampled bores were suitable, i.e. do not leak groundwater from shallower aquifers.
- This multi-tracer study allowed determining flow velocities in the deeper Precipice, which are astonishingly high.
- This study allowed the first quantitative estimate of recharge into the Precipice Sandstone.
- The double porosity model for the Hutton Sandstone was confirmed as are the recharge estimates derived in (Suckow *et al.* 2016).
- Present day state of the art flow and reactive transport modelling can now use three different tracer systems as calibration target (^{14}C, $^{36}Cl/Cl$ and helium) to quantify fluxes in the Hutton and Precipice Sandstone with higher confidence.

were then evaluated to discuss their aquifer-specific spatial pattern and infer the horizontal groundwater velocities. In this aquifer-specific discussion we start with the Precipice sandstone because this report is the first comprehensive tracer study in the Mimosa syncline in this aquifer. There was only 10% new data for the Hutton Sandstone and therefore the discussion for the Hutton Sandstone is mainly discussing how the new findings provide confirmation of the earlier assessment (Suckow *et al.* 2016).

3.1   Tracer cross plots and depth profiles

Tracer-tracer cross plots and depth profiles of the tracer data aimed to: 1) evaluate the presence of 'young' groundwater (<60 years); 2) determine the initial ^{14}C activity at recharge; 3) determine the initial ^{36}Cl to Cl ratio ($^{36}Cl/Cl$) at recharge and 4) give valuable information for a first qualitative synthesis of the data. The cross plots and depth profiles are discussed qualitatively for both aquifers together, providing underpinning evidence to the more qualitative and preliminary conclusions later.

3.1.1 ^{14}C-^{3}H:

The recent sampling campaign had a special focus on the recharge areas of Hutton and Precipice, where the youngest waters are expected and initial conditions of ^{14}C and $^{36}Cl/Cl$ are defined. Nevertheless, also the new results for the Hutton Sandstone show no tritium (^{3}H) in the cross-plot with ^{14}C (Figure 3.1). The detection limit for the last two campaigns is in the range of 50-60mTU (milli TU), which corresponds to 2% of recent rain having 2-3TU (Tadros *et al.* 2014). The earlier analytical detection limit for the GA and GABWRA datasets, also included in Figure 3.1 was 0.25 TU, corresponding to 10% recent rain. In the Hutton Sandstone the shallowest bore (RN 16836) has a screen from 11.6 to 24.4 m below ground. Finding no tritium (<2% recent rain) in this well implies that the water down to 24.4 m is older than 1960. Since this well was sampled in 2011, the water is older than 50 years and the vertical distance velocity is smaller than 0.5 m/y. Assuming a porosity of (22±6)% (Smerdon and Ransley 2012), this implies recharge is less than 80 mm/y to 140 mm/y. A similar calculation for the Precipice, where the shallowest sampled bores (RN89724 & RN89889) have screens below ground of 65 m to 89 m and 76 m to 88 m and were sampled in 2017, gives values of less than 1.5 m/y for the distance velocity and with the porosity of (16±5)% (Smerdon

and Ransley 2012) give recharge of less than 165-350 mm/y. It would have been desirable to find a shallower bore in the Precipice recharge area, but none was available for this study.

Another valuable result of the tritium measurements is that the radiocarbon samples are not mixed with recent groundwater and bomb-radiocarbon in the samples is insignificant. It also gives no indication of any well leakage (that is, infiltration of rainwater or shallower groundwater along the well casing). Regional initial ^{14}C values seem to be higher than 75% in the Precipice Sandstone and higher than 80% in the Hutton Sandstone, but cannot be more precisely quantified.
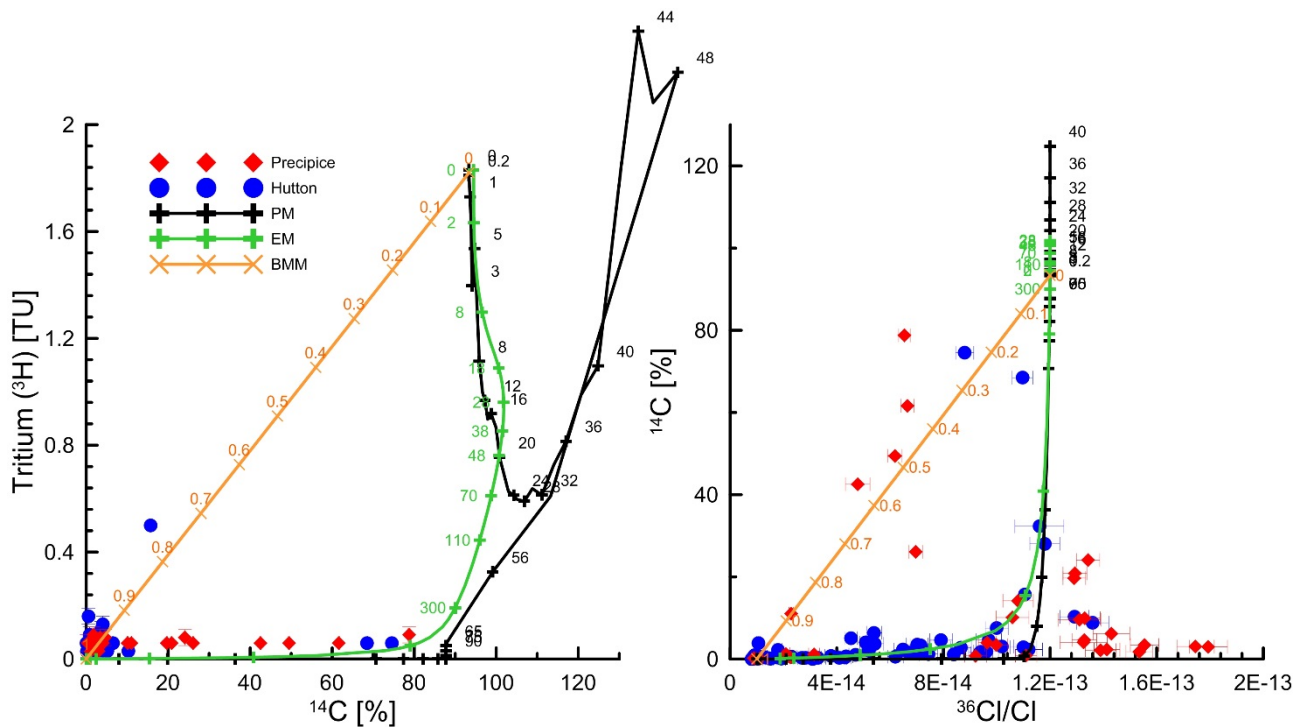
Figure 3.1: Plot of ^{3}H versus ^{14}C (left panel) and ^{36}Cl/Cl versus ^{14}C (right panel) for the Hutton and Precipice Sandstone aquifers. Lumped parameter models (PM, EM, BMM) are shown for comparison. Numbers on the models are mean residence times (MRT) for PM & EM and mixing ratios for BMM.

3.1.2 ^{14}C-^{36}CL/CL:

The highest and lowest measured radiocarbon values in the Precipice Sandstone and in the Hutton Sandstone are 74.5% and 0.12% and 78.75% and 0.13%, respectively. The lower values here may be regarded as practical detection limit: while the analytical detection limit of AMS systems is considerably lower, it is hard to generate a groundwater sample that has less than 1 permil signature of modern water. The highest and lowest measured ^{36}Cl/Cl values in the Precipice Sandstone and in the Hutton Sandstone are $1.8 \cdot 10^{-13}$ and $8.85 \cdot 10^{-15}$ and $1.4 \cdot 10^{-13}$ and $8 \cdot 10^{-15}$, respectively. Also here the lowest values correspond to the practical limit: underground production resulted in an equilibrium around $1 \cdot 10^{-14}$ in groundwaters from the Hutton Sandstone (Suckow *et al.* 2016) and similar values are expected for the Precipice Sandstone.

High values in ^{14}C are not correlated with high values in ^{36}Cl/Cl in the Precipice Sandstone, which is an unexpected result in Figure 3.1 (right panel): those samples with high ^{14}C have intermediate ^{36}Cl/Cl values and vice versa. The highest values of ^{36}Cl/Cl are in the Precipice Sandstone and in waters that according to face value ^{14}C interpretation would be several thousand years old. The most probable explanation is that there was a higher input of ^{36}Cl/Cl in the recent geological history than today, probably during the last glaciation. This will be discussed further below.

Plotted as depth profile, the radiocarbon concentrations decrease more rapidly with depth in the shallower Hutton Sandstone than in the underlying Precipice Sandstone aquifer (Figure 3.2 left panel). In the Hutton Sandstone, all radiocarbon samples below 600 m depth are below 1%, most of them at the detection limit. In contrast, in the Precipice Sandstone only four samples below 800 m depth have less than 1% in ^{14}C, most

of them are clearly above the detection limit. This indicates a much higher flow velocity and recharge in the Precipice Sandstone than in the Hutton Sandstone. We do not intend interpreting depth profiles to quantify recharge, since these depth profiles are a composite of 60 km flow distance.

The difference in penetration of natural radioactive tracers into the two aquifers is even more pronounced for ^{36}Cl/Cl. In Hutton Sandstone all samples below 600 m depth were at secular equilibrium with underground production (Suckow *et al.* 2016). In contrast, the highest ^{36}Cl/Cl values in the Precipice Sandstone and the Mimosa Syncline as a whole were found at depths of 570 m and 1033 m. Only two samples from the Precipice Sandstone are at secular equilibrium of underground production, and these are from wells deeper than 1000 m. If one neglects a group of six samples most of which are at the very end of the flow path and East of the Burunga-Leichardt Fault (see below), there is actually no clear decrease of ^{36}Cl/Cl discernible with depth. This means that groundwater in the Precipice Sandstone within the sampled area of the Mimosa Syncline (ca. 170 km of flow distance) circulates on time scales faster than a few hundred thousand years, and taking ^{14}C into account, probably in large parts faster than 50 ky.

Comparison of the trends in ^{14}C and ^{36}Cl/Cl can also be used to evaluate the initial ^{36}Cl/Cl of groundwater entering the aquifers (Figure 3.1). Compared to the earlier report, (Suckow *et al.* 2016), we have now some Hutton Sandstone groundwater samples with higher ^{14}C. Compared with the Precipice Sandstone, the Hutton Sandstone groundwaters containing ^{14}C show a comparably narrow range in ^{36}Cl/Cl (2–14·10^{-14}). When interpreted with LPMs, the ^{14}C/^{36}Cl data of Hutton Sandstone can be fitted either with a PM or EM model but not with a BMM model (Figure 3.1 right panel), therefore excluding significant mixing of water with very different age. Based on samples with relatively high ^{14}C, originating from closer to recharge areas, the initial ^{36}Cl/Cl in recharge would be ~1.2·10^{-13}. Initial ^{36}Cl/Cl is much more difficult to define for the Precipice, because samples with detectable ^{14}C show a broader value of 5·10^{-14} to 1.8·10^{-13}. Some of these data points seem to lie on a mixing line, some outside the range defined for the Hutton Sandstone and it is hard to describe them with a simple lumped parameter approach. One possible explanation is that ^{36}Cl/Cl was not constant during the hydrological history accessible by ^{14}C (that is: the last 40 ky).
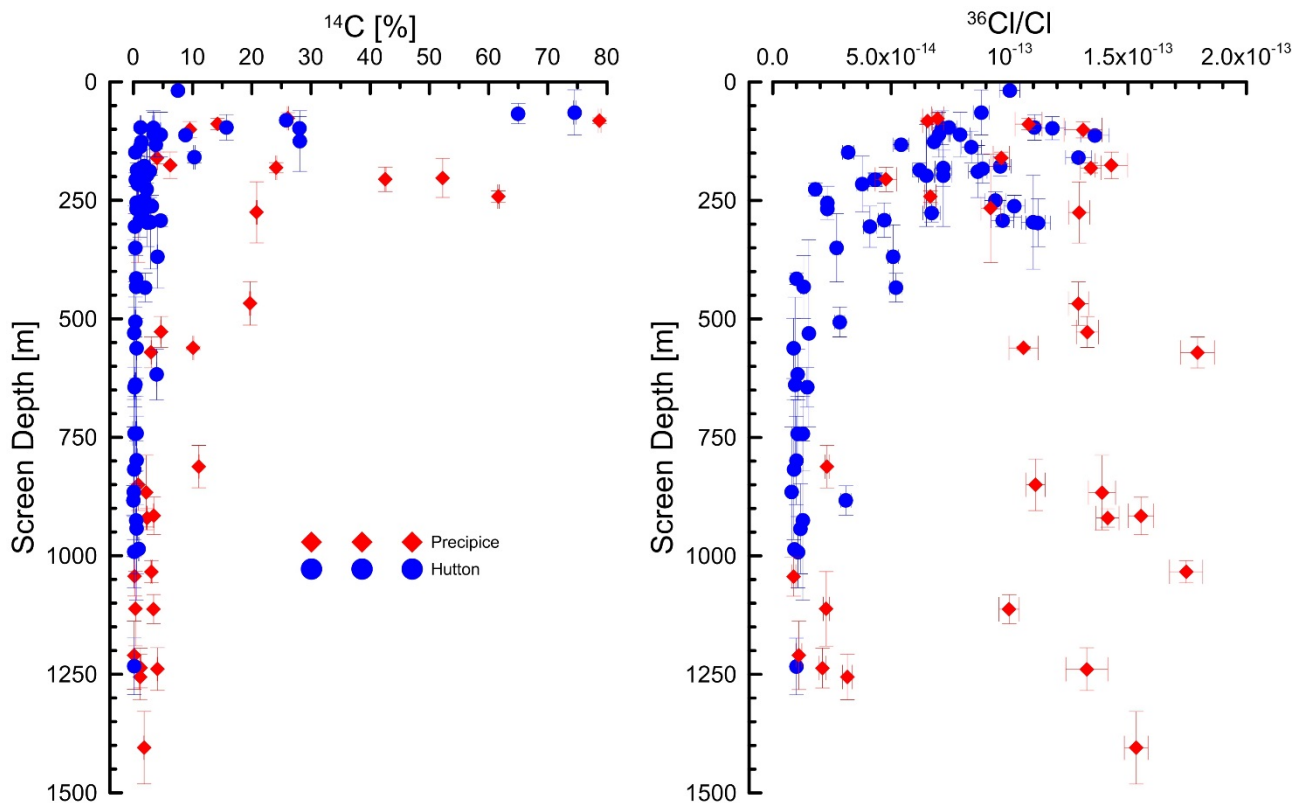
Figure 3.2: Depth profiles of ^{14}C and ^{36}Cl/Cl.

3.1.3 STABLE ISOTOPES OF WATER (^{18}O & ^{2}H)

Stable isotopes of water had previously been interpreted as climate indicators on the basis of flow velocity in the Hutton Sandstone (Suckow *et al.* 2016). Plots of ^{2}H versus ^{14}C and versus $^{36}Cl/Cl$ are presented in Figure 3.3. The trend for ^{18}O is identical to ^{2}H and not shown here. The most negative values (<-40‰ to -50‰ in ^{2}H) are at secular equilibrium in $^{36}Cl/Cl$ and mostly below 1% in ^{14}C. Those samples that have measurable ^{14}C are all from the GABWRA dataset and one of them is even young in ^{14}C (RN58432 has 52%, sampled in May 2009). Stable isotope values are much more negative in the Hutton Sandstone than in Precipice Sandstone and the most negative values of (<-40‰ in ^{2}H) are found at depths between 300 m and 1200 m.
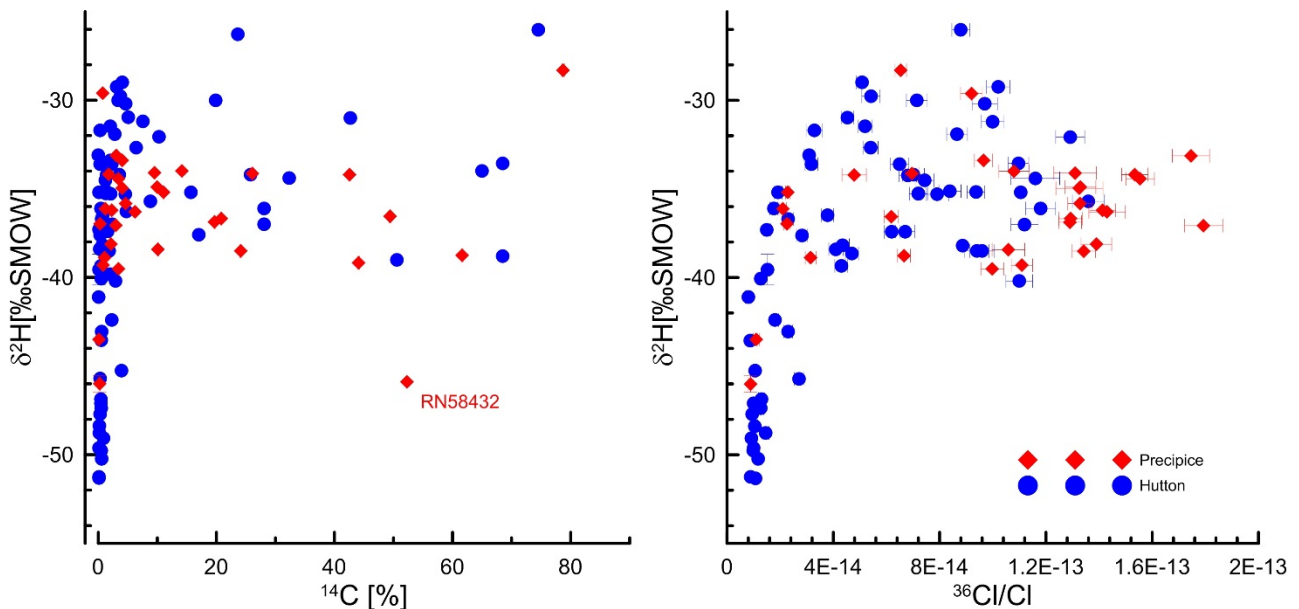
Figure 3.3: Tracer cross plots of ^{2}H versus ^{14}C (left) and $^{36}Cl/Cl$ (right) for Hutton Sandstone and Precipice Sandstone

The previous interpretation by (Suckow *et al.* 2016) that the negative stable isotope values may correspond to the last glaciation cannot be kept in view of the new data. Also the samples from Precipice Sandstone reach times as old as the Last Glacial Maximum (LGM – between 17-20 ky, (Barrows *et al.* 2002)). This can be concluded from the decrease of radiocarbon (Figure 3.1) and because the flow velocities needed to cross the whole sampled area (60 km flow distance) within less than 10 ky (or more than 6 m/y) are not reasonable in this hydrogeological system. Furthermore, there is no clear shift in stable isotope composition discernible that would agree to stable isotope patterns observed in other aquifers around the world as palaeoclimate signal. And without a groundwater palaeoclimate signal in the Precipice, a palaeoclimate signal in the Hutton Sandstone is not very likely, given that its infiltration area is only a few tens of km south of the Precipice infiltration beds (Figure 2.4). All groundwater samples discussed in (Suckow *et al.* 2016) that have a "Pleistocene" stable isotope signature in the Hutton Sandstone, have their ^{14}C and $^{36}Cl/Cl$ values at the detection limit or at secular equilibrium, respectively. This means these waters can be much older than the LGM.

3.1.4 HELIUM AND HEAVIER STABLE NOBLE GASES

As a general consistency check the heavy noble gases (Ne, Ar, Kr, Xe) and N_2 are plotted against each other. Theoretically a total of ten binary plots are possible, of which only two are shown in Figure 3.4. The assessment of the heavy noble gases then gives information about the infiltration conditions, which often contains palaeoclimate information and also indicates the reliability of the helium measurements.

Figure 3.4: Noble gas cross plots for xenon versus neon (left) and xenon versus krypton (right) for Hutton Sandstone and Precipice Sandstone. Numbers on the black solubility equilibrium line correspond to recharge temperatures.

Heavy noble gases

The black line in Figure 3.4 shows the solubility equilibrium of a pair of noble gases at varying temperatures from 0°C to 50°C. Temperature dependence is largest for xenon (ne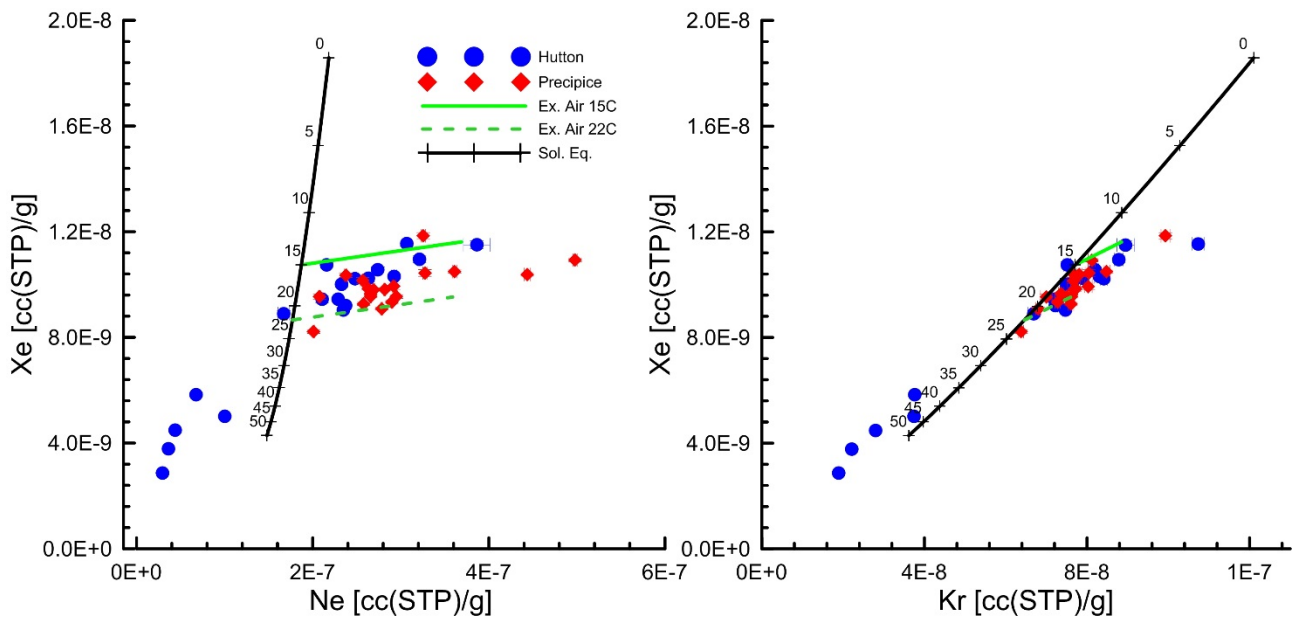arly factor of five) and smallest for neon (factor 1.3), which is why the range of the black line for xenon is longer than the one for neon and krypton (factor 3). The two green lines add up to 0.01cc/g excess air (Heaton and Vogel 1981) to the equilibrium concentrations at 15°C and 24°C. The effect of excess air is largest for neon and smallest for xenon. The binary noble gas plots therefore confirm that infiltration temperatures for most samples varied between 15°C and 24°C.

A few samples are out of this pattern and fall below the concentration values for solubility equilibrium (left and below the black line in Figure 3.4). These are the samples from the wells RN123444, Reedy Creek INJ3-H, RN15508A, Carinya MB5-H, Talinga MB3-H, RN58409A and RN89889. These samples contain less noble gases than can be explained by solubility equilibrium, and the noble gas deficiency is larger for the lighter noble gases. That is: the deficiency is larger for Ne than for Xe. Such a pattern occurs when degassing of the groundwater happens – either during sampling or in the aquifer itself. Degassing in the aquifer may happen for instance in areas of strong biogenic CO_2 production or strong (e.g. fertilizer-driven) de-nitrification. In these cases the effervescing gas strips noble gases from solution as well, a process well documented in the literature (e.g. (Visser *et al.* 2007; Visser *et al.* 2009). However, this process can be excluded here, since the samples were taken from >500 m depth. In the present case this degassing is caused by de-pressurizing the groundwater during pumping to the ground surface. In two cases (Carinya MB5-H and Talinga MB3-H) also pumps were used that are not suitable for noble gas sampling (Airwell Pumps). These pumps operate with compressed air and create a direct contact between the compressed air and the groundwater at depth – typically screen depth or several tens of meters below the water table. This compressed air enters the groundwater by dissolution (100 m depth correspond to 10 bar partial pressure of compressed air at equilibrium) and effervesces when the groundwater is ascending in the pump tube. Degassing was clearly visible while sampling the wells Carinya MB5-H and Talinga MB3-H. Another possibility is that the groundwater is naturally supersaturated with gas at ground pressure. That is: the total dissolved gas pressure is significantly higher than one atmosphere, for instance due to dissolved methane in the groundwater. In this case special sampling equipment need to be applied in an open borehole to obtain an undisturbed noble gas sample (Banks *et al.* 2017). However, it was not possible to realize this sampling situation in the present cases, since all sampled wells were equipped with pumps, either from the landholder or from the industry. Therefore, the heavy noble gas concentrations for the Hutton bores RN123444, RN15508A, Carinya MB5-H, Talinga MB3-H, RN58409A cannot be evaluated and also the

measured helium concentration for these samples is probably significantly lower than in situ in groundwater. In the following plots these samples are marked with a black circle around the measured value.

Helium

Maximum helium concentrations are $8.3 \cdot 10^{-5}$ cc/g in the Precipice and $7.3 \cdot 10^{-5}$ cc/g in the Hutton Sandstone, and the measured minimum concentration corresponds to solubility equilibrium ($4.5 \cdot 10^{-8}$ cc/g at 20°C). The plot of ^{4}He versus ^{14}C confirms the expected trend that high helium is correlated with low ^{14}C, both directions indicating older water (Figure 3.5, note that the axes in these plots are oriented such that "old" is the direction to upper right). From this plot of helium versus ^{14}C (Figure 3.5 left panel) for the Precipice an ingrowth rate for ^{4}He of roughly $5 \cdot 10^{-10}$ cc/(g y) describes most of the data (blue line in left plot). This is a very high value, much higher than expected from in-situ production from uranium and thorium alone (Smith 2015). Our data indicates that the helium ingrowth is smaller for younger waters compared to this trend, and larger for older waters (red and blue dots fall below the blue line for high ^{14}C and above for low ^{14}C). This is in agreement with earlier findings in the GAB (Torgersen and Clarke 1985; Torgersen and Ivey 1985; Torgersen and Clarke 1987) and describes how the groundwater takes up an external helium flux ("crustal helium flux").

There is not much indication of mixing from the binary plots of helium and radiocarbon in the Precipice (the binary mixing line of old and young water is indicated by the BMM model, yellow curve in Figure 3.5). In the Hutton Sandstone, the samples from the Amusen, Dangarfield and Moorabinda wells are characterized as mixtures with high helium and comparably high ^{14}C. Ingrowth of helium within the Hutton is in a similar order of magnitude as in the Precipice Sandstone, when using ^{14}C as benchmark.
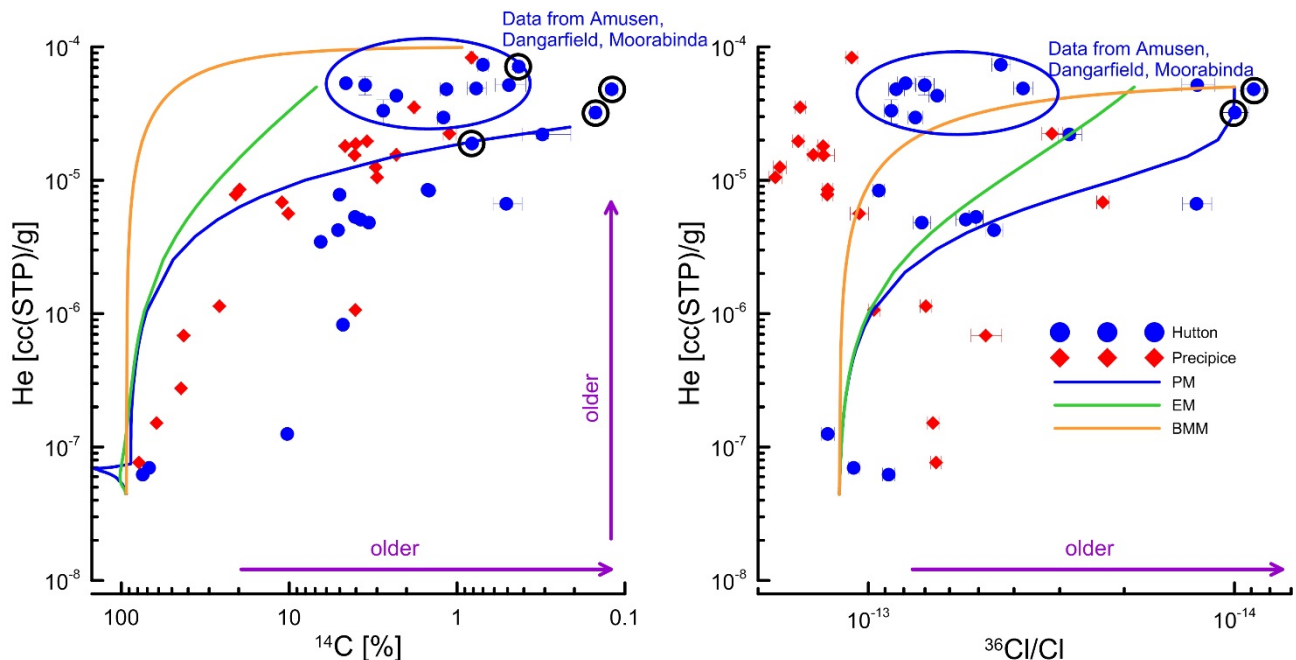
Figure 3.5: Measured helium concentration versus ^{14}C (left) and versus ^{36}Cl/Cl (right) for Hutton Sandstone and Precipice Sandstone

The plot of ^{4}He versus ^{36}Cl/Cl gives again clear indication of groundwater mixing for some samples in the Hutton Sandstone, by having high ^{36}Cl/Cl ratios and high helium concentrations and lying close to the binary mixing model (BMM). These samples were identified in (Suckow *et al.* 2016) already as originating from the farms Amusen, Dangarfield and Moorabinda, and are probably influenced by old water with high helium concentrations ascending along the Hutton Wallumbilla fault. In the Precipice Sandstone aquifer most samples have high ^{36}Cl/Cl ratios as discussed above. Also here the highest ^{36}Cl/Cl ratios are correlated with

high ^{4}He concentrations (between $1 \cdot 10^{-5}$ and $1 \cdot 10^{-4}$cc/g). The helium results thereby also characterize these waters as old, as did ^{14}C. An approximate production line to the remaining samples of the Precipice Sandstone would suggest a He production more like $1 \cdot 10^{-11}$cc/(g y), which is a factor of 50 smaller than derived from ^{14}C. Qualitatively higher in-situ production rates in the Hutton Sandstone would be expected due to the double porosity system that the Hutton Sandstone represents: the stagnant layers remove ^{36}Cl/Cl more effectively and supply ^{4}He more effectively by diffusion from the stagnant into the mobile zones than in the Precipice Sandstone. The fact that the helium values are higher in Precipice Sandstone for samples with higher ^{14}C (younger) is attributed to the Precipice being deeper and therefore first in receiving crustal helium flux from below.

For future activities in this area it is suggested to include measuring the isotope ratio ^{3}He/^{4}He as well. This can indicate how the terrigenic helium is produced and whether the origin is from the mantle (higher ^{3}He/^{4}He) or from crustal production (low ^{3}He/^{4}He) (Ballentine *et al.* 2002).

Plotting the stable isotopes of water versus the helium concentration (Figure 3.6) again demonstrates that the most negative isotope values (<-45‰ in ^{2}H) are correlated with highest helium concentrations, indicating oldest age.

In the Precipice Sandstone helium concentrations increase quite linearly with depth (Figure 3.6), at a rate of $1.7 \cdot 10^{-8}$cc(STP)/g per meter depth. The rate for the Hutton Sandstone is similar at $3 \cdot 10^{-8}$cc(STP)/g per meter depth, if one neglects the group of samples at the farms Amusen, Dangarfield and Moorabinda. The latter have high helium concentrations at shallow depths and indicate ascending water along the Hutton Wallumbilla fault (Suckow *et al.* 2016).
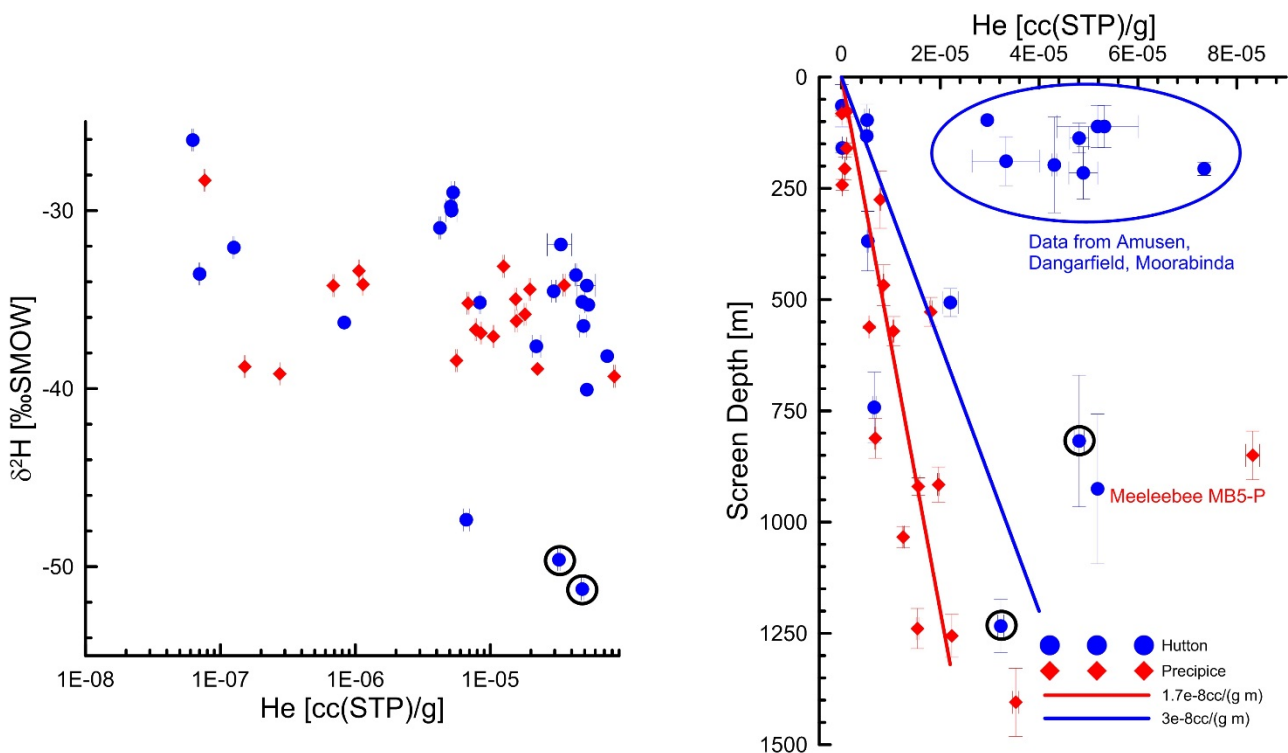
Figure 3.6: Stable isotopes (^{2}H only) versus ^{4}He (left) and depth profile of helium (right) for Hutton Sandstone and Precipice Sandstone

3.1.5 DEPTH PROFILES FOR CHEMICAL PARAMETERS

For the interpretation of ^{14}C and ^{36}Cl/Cl the chemical characterization of the groundwaters in terms of total dissolved inorganic carbon (TDIC = alkalinity expressed as mMol/L carbon) and stable chloride concentrations are of importance. Increases in TDIC and Cl$^-$ dilute the ^{14}C and ^{36}Cl/Cl signals, respectively, without any radioactive decay, hence it distorts the "age" signal chemically towards older.

TDIC increases with depth in Hutton Sandstone at a rate between 9μMol/L and 23μMol/L per meter depth (Figure 3.7). TDIC hardly increases with depth in groundwaters from the Precipice Sandstone. For the three exceptional samples TDIC correlates with high Cl concentrations and these are situated east of the Burunga-Leichardt fault and south of Miles, Chinchilla and Dalby. Besides these exceptional samples with high chloride concentration, Cl^- is quite constantly low in Precipice Sandstone over the whole depth range sampled (<100 mg/L). In the Hutton there is a general trend of increasing Cl^- with depth that can be quantified between 0.125 mg/L and 0.67 mg/l per m depth (lines in Figure 3.7, please note the broken axis with two different increases below and above 600 mg/L). Exceptions to this trend are again the waters close to the two fault systems.
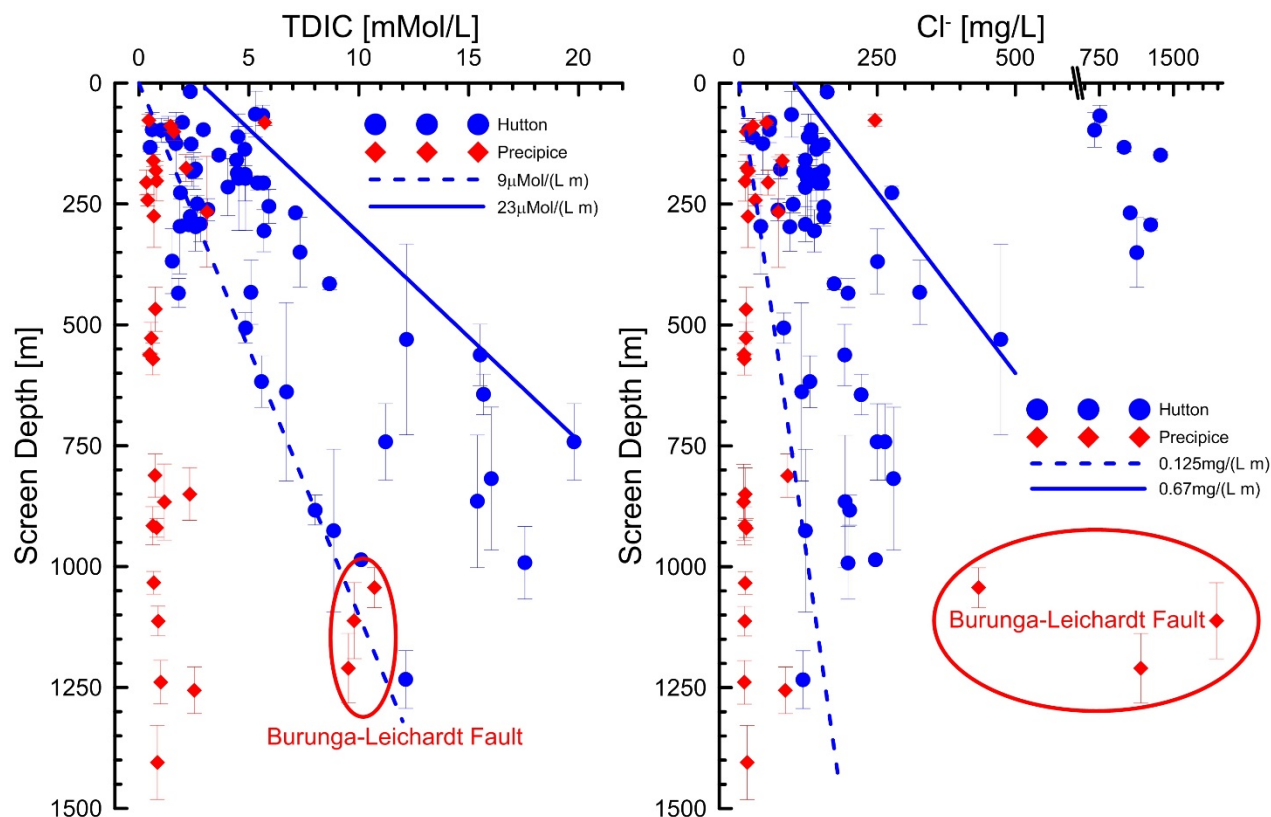
Figure 3.7: Depth profiles for Total Dissolved Inorganic Carbon (TDIC) (left) and Cl⁻ (right) for Hutton Sandstone and Precipice Sandstone

3.2   Regional tracer distribution and transects along flow direction

This section discusses the regional tracer distribution using maps of the single tracers and how the tracer development looks like along the flow paths from the infiltration area into the deeper aquifer. The distance relationship will again be the shortest distance to the outcrop of the formation (Hutton Sandstone and Precipice Sandstone respectively), as discussed in (Suckow *et al.* 2016). For maps of chloride concentrations we refer to the report of (Raiber and Suckow 2017).

3.2.1   PRECIPICE SANDSTONE

Prior to this study, the Precipice Sandstone in the Mimosa syncline was basically unchartered territory. The earlier report of (Suckow *et al.* 2016) doubled the number of existing measurements and had a dataset of eight samples for ^{14}C and [36]Cl/Cl available in the Mimosa Syncline. After the present study a total of 34 and 31 values are available in the Precipice Sandstone for ^{14}C and [36]Cl/Cl respectively, which allows regional patterns to be described.

TDIC as well as Cl⁻ are low and comparably constant with flow distance in the Precipice Sandstone (Figure 3.9), increasing only at a rate of (8 to 80) µMol/L per meter of flow and (60 to 800) µg/L per meter of flow for TDIC and Cl⁻ respectively. These rates are approximately a factor 100 lower than for the Hutton Sandstone (Suckow *et al.* 2016). This implies that there is hardly any dilution of ^{14}C and ^{36}Cl by "dead" carrier TDIC and Cl⁻, respectively, and no indication that ^{14}C and ^{36}Cl/Cl ratios cannot be used to infer advective distance velocities in the Precipice Sandstone. In Precipice Sandstone groundwaters ^{14}C is also clearly detectable in the confined area away from the outcrop and south of the Dawson River (Figure 3.8 top). The measured ^{36}Cl/Cl ratios are even higher south of the Dawson River than north of it (Figure 3.8 bottom). This clearly indicates that flow in the Precipice Sandstone does not end at the Dawson River to discharge, but extends into the deeper parts of the aquifer.

From the transect of radiocarbon versus distance to outcrop in Precipice Sandstone an advective distance velocity of 0.8-1.5m/y can be derived (Figure 3.10 left panel). This distance velocity is not in contradiction to the ^{36}Cl/Cl findings. However, it can also not be better quantified by ^{36}Cl/Cl, because radioactive decay[1] is not yet clearly visible on this transect (Figure 3.10 right panel). The question is, however, why the scatter of ^{36}Cl/Cl values in Precipice is comparably large for the "young" samples, that is: for samples that contain ^{14}C. These range from $4.8 \cdot 10^{-14}$ to $1.8 \cdot 10^{-13}$ which is more than a factor of three, as compared to less than a factor of two in the Hutton (Figure 3.1 right panel).

The values of the stable isotopes of water cannot shed much light on this question because they are quite homogeneous along the transect and on the spatial distribution (Figure 3.11 top). The distribution of ^{4}He in this case seems to be a better indicator (Figure 3.11 bottom). Helium is low in the recharge areas of Precipice and seems to increase rapidly up to a travel distance of 20km, then remains fairly constant; the rate of increase along the flow path is $4 \cdot 10^{-10}$ cc(STP)/g per meter flow distance (Figure 3.12). The samples with exceptionally high ^{36}Cl/Cl ratios (>1e-13) have comparably high helium concentrations which characterizes them as several thousand years old. If we therefore exclude mixing of very old and younger waters – for which up to now we do not have good indications – then the large range of ^{36}Cl/Cl values seen in Figure 3.10 (right panel) is most probably created by secular input variations – may that be variations in cosmogenic production of ^{36}Cl or from variations of Cl⁻ input from sea-spray due to palaeoclimatic influence on wind fields or proximity to the ocean.

Recharge estimate

We are not aware of earlier estimates of deep recharge into the Precipice Sandstone. Conclusive estimates were done on the GAB aquifers such as Gubberamunda Sandstone and Hutton (Smerdon and Ransley 2012) or detailed methodological comparisons for the Surat Basin as a whole (Reading *et al.* 2016), but these gave no quantitative estimates for deep recharge to the Precipice Sandstone. The distance velocity we derived here from the ^{14}C transect is used for such an estimate, since it is not in contradiction to any other tracer finding. If we use the mean porosity of the Precipice Sandstone of (16±5)% (Smerdon and Ransley 2012) then the distance velocity of 0.8-1.5 m/y results in values for the Darcy velocity of 110 mm/y to 315 mm/y. One of the uncertainties in this approach may be seen in the way how the distance was determined (Suckow *et al.* 2016): since the distance here is defined as the shortest land surface distance between the outcrop area and the well, the distance is probably slightly underestimated because of a more tortuous path the water would take in the real world. Which would imply the real value for the distance velocity may be higher. On the other hand, any preferential flow path that uses only the part of the porosity distribution with high porosity (and transmissivity) would also influence the calculated Darcy velocity – and again the calculated value above would be too small, since the real, effective porosity would be higher.

Another question is how these values for the distance and Darcy velocity can be re-calculated into a water balance for the Precipice as a whole: The total outcrop area of Precipice Sandstone between 149 and 150.5 degrees longitude can be easily determined with a Geographical Information System (GIS) as 1255 km². Multiplying the range of Darcy velocities above with this area results in a total recharge estimate into the

---

[1] With a half-life if 301,000 years, little decay has happened in the time frames considered here (couple of ten thousand years)

Precipice Sandstone of 135 GL/Y to 395 GL/y. This would be more than tenfold the amount of earlier chloride mass balance (CMB) recharge values to the Hutton Sandstone (Suckow *et al.* 2016) and higher than the total recharge into the Gubberamunda in the Surat Basin, which was estimated between 157GL/y and 295GL/y (Habermehl *et al.* 2009; Smerdon and Davies 2012) and therefore this calculation is not realistic.

Since the distance velocities are calculated versus flow distance, the most correct area to multiply the abovementioned range of Darcy velocities with, for obtaining a total recharge amount, would be the cross-sectional area perpendicular to the flow direction. In practice this is the average thickness of the formation (Precipice Sandstone) multiplied with the length of this cross section. We evaluated the formation thickness of the Precipice Sandstone in those bores that completely penetrated the Precipice Sandstone and found a range of 40 m to 130 m thickness. From this assessment we estimate the average thickness to be (85±10) m. Multiplying this thickness with the length of the Hutton recharge area of 226 km used earlier ((Suckow *et al.* 2016), Figure 4.1) gives a total cross section area of (19±2) km^2. However, one could also argue for a cross section of only 120km length, which corresponds to the straight distance between the southmost tips of the outcrop of the Precipice Sandstone in the Mimosa Syncline. This would result in a cross-sectional area of (10.2±1.2) km^2. In summary this leads to a more realistic range of total recharge for the Precipice Sandstone of 1.1 GL/y to 6.6 GL/y in the Mimosa Syncline area.
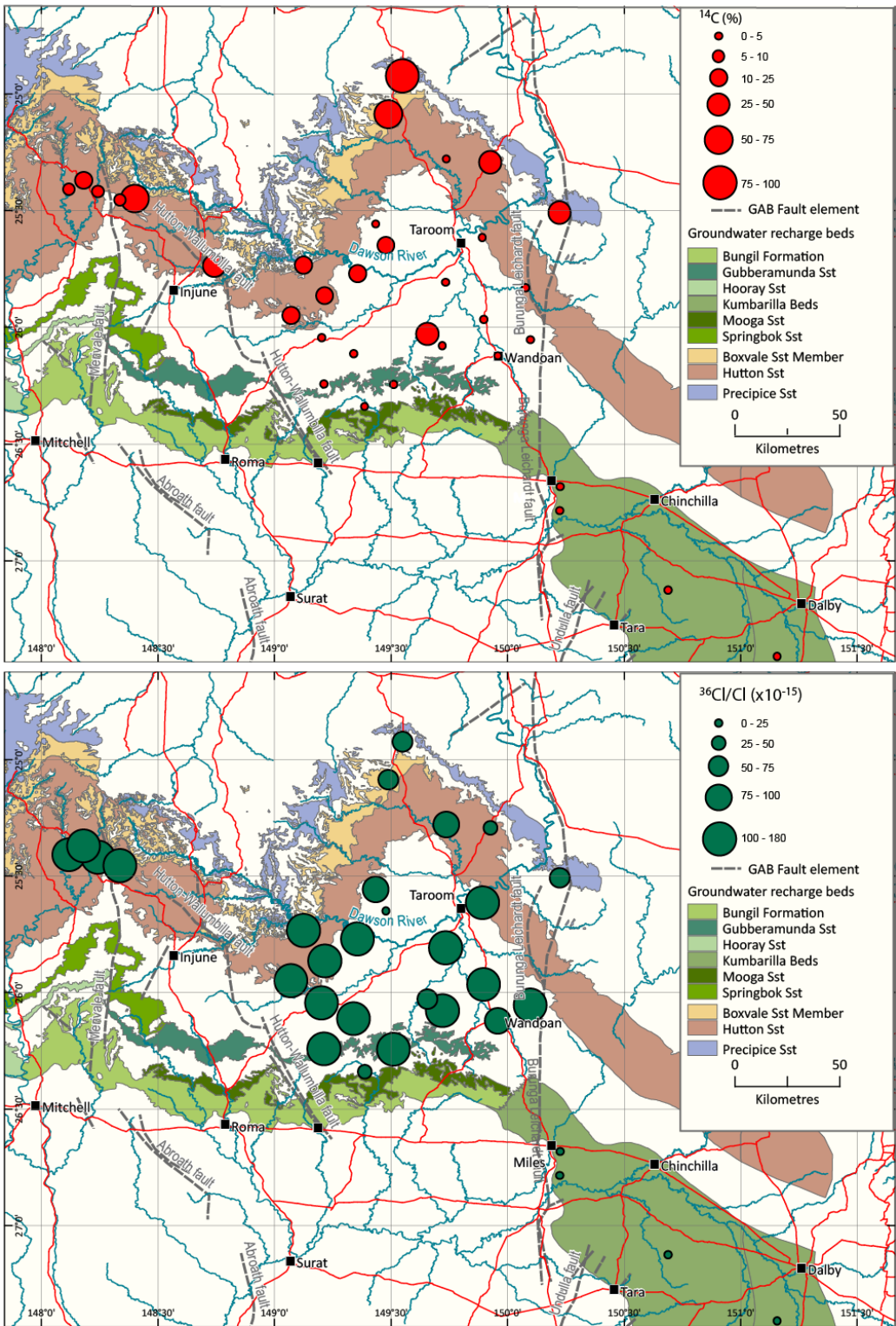
Figure 3.8: Map of ^{14}C values (top) and ^{36}Cl/Cl values (bottom) in the Precipice Sandstone.

Figure 3.9: Transect of Total Dissolved Inorganic Carbon (TDIC, left) and Cl⁻ (right) for the Precipice Sandstone

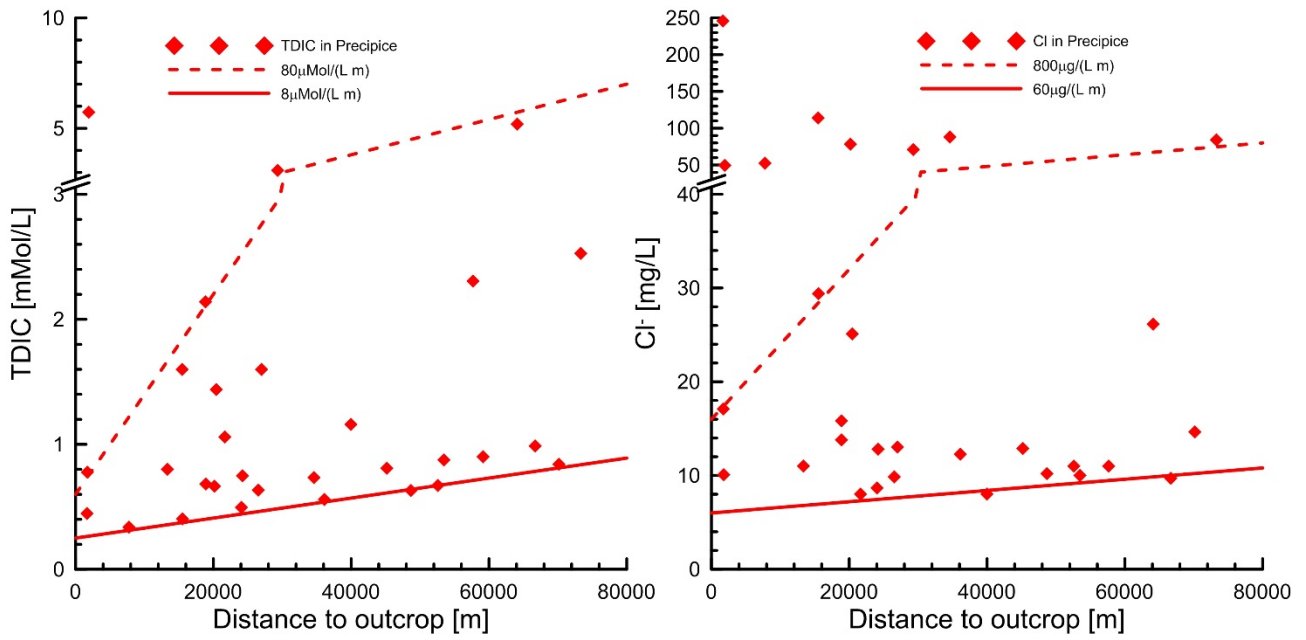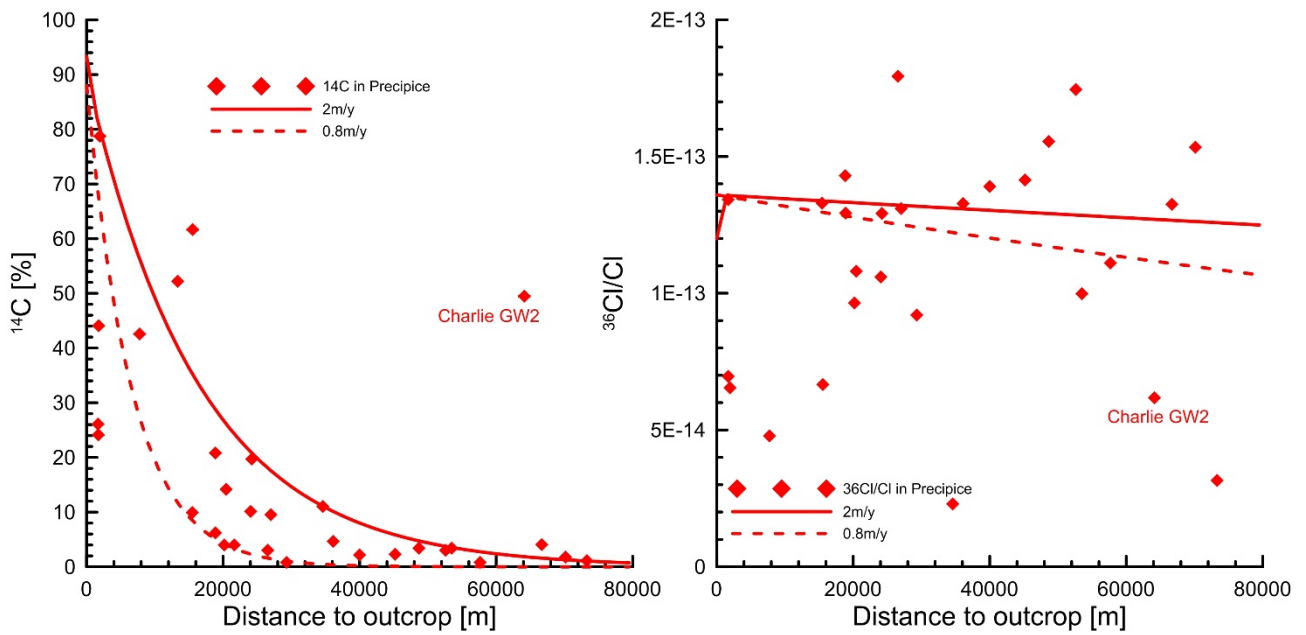**Figure 3.10: Transect of radiocarbon (¹⁴C, left) and ³⁶Cl/Cl (right) for the Precipice Sandstone**
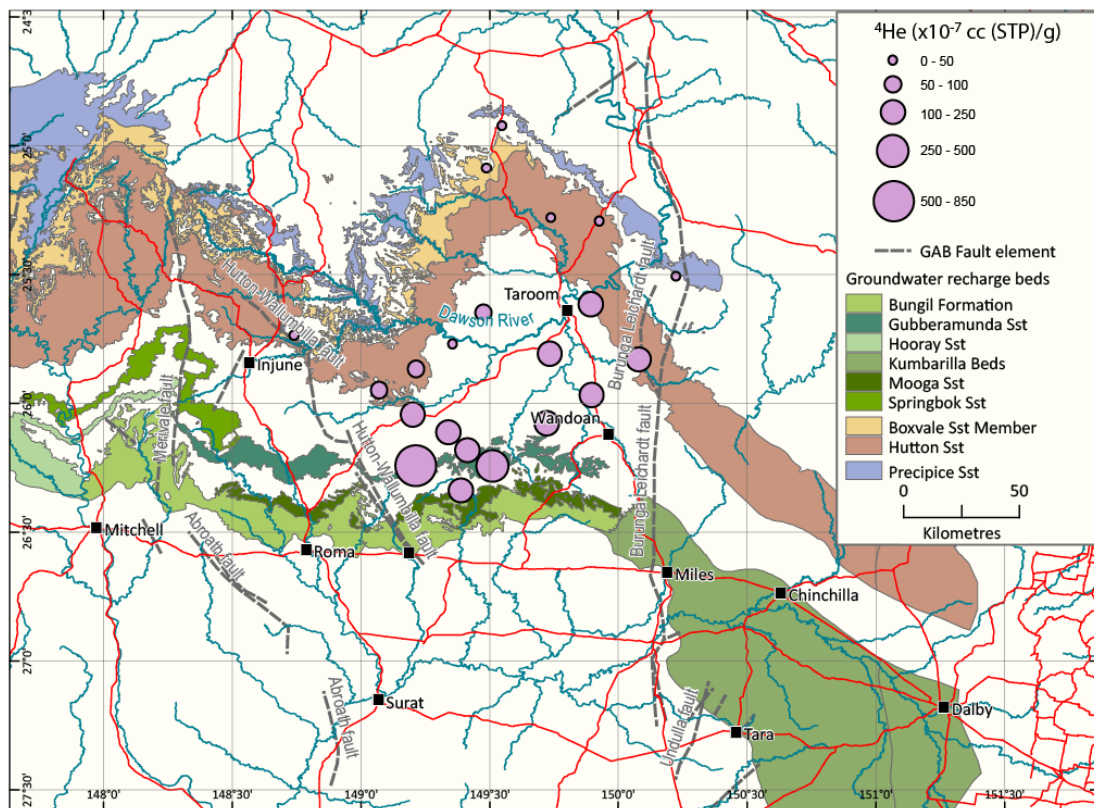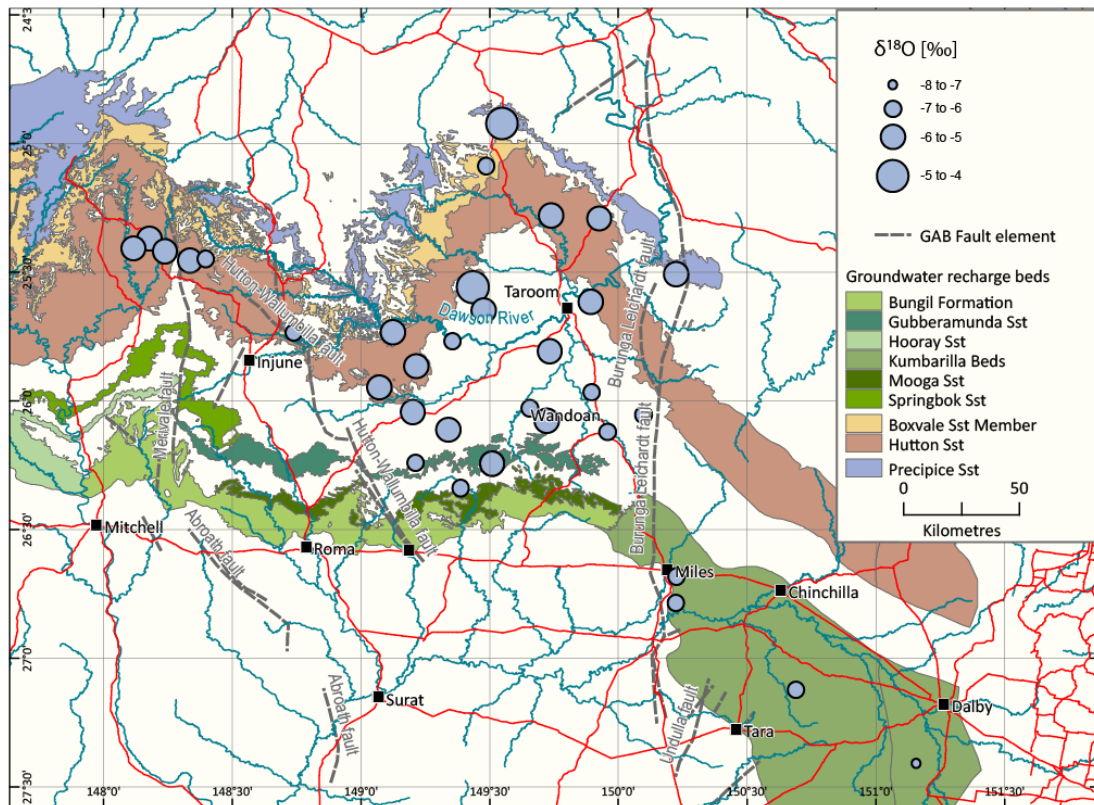
Figure 3.11: Map of ^{18}O values (top) and ^{4}He concentrations (bottom) in the Precipice Sandstone.
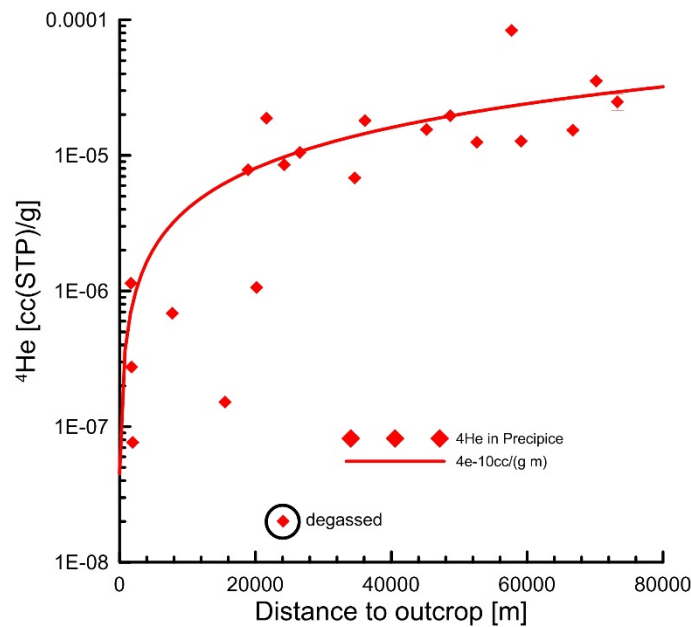
Figure 3.12: Transect of helium for the Precipice Sandstone

3.2.2 HUTTON SANDSTONE

The present study allowed assessment of some extra samples in the infiltration areas, and confirms that ^{14}C is present in Hutton Sandstone basically only in the outcrop areas of the Hutton (Figure 3.13 top). As soon as the Hutton Sandstone is confined, ^{14}C drops to values smaller than 10%. ^{36}Cl/Cl in contrast penetrates into the confined part of the aquifer but the high values seem to be restricted to the areas north and west of the main branch of the Dawson River (Figure 3.13 bottom). An exception to this trend is the southwest part of the flow system, where ^{36}Cl/Cl stays higher in flow direction towards Wallumbilla. East of 149.4 longitude, south of Wandoan and west of the Burunga Leichardt fault all ^{36}Cl/Cl values in the Hutton Sandstone are at secular equilibrium. This confirms earlier assessments (e.g. (Hodgkinson *et al.* 2010; Raiber and Suckow 2017) that the flow system of the Hutton Sandstone reaches only to the Dawson River and is then discharged.

The stable isotope data (only ^{18}O shown in Figure 3.14) confirm this finding in so far as the most negative values occur in waters that are in secular equilibrium with ^{36}Cl/Cl. Also this indicates that the flow system may be restricted to the area north of the Dawson River. However, the helium concentrations (Figure 3.14 bottom) do not increase drastically in the old waters with very negative signature in stable isotopes and secular equilibrium signature in ^{36}Cl/Cl. It may well be that the additional helium produced in these waters is exported to overlying layers via molecular diffusion. This will be demonstrated in the numerical transport studies within this project.

In transects along the flow distance the additional data confirm the earlier trends: TDIC and Cl$^-$ increase with flow distance in the Hutton Sandstone. However, this increase and the corresponding dilution of the ^{14}C and ^{36}Cl/Cl ratios with "dead" (non-radioactive) carbon and chloride cannot explain the discrepancy between the tracer-derived flow velocities. A double porosity system as described by (Sudicky and Frind 1981) is needed to explain both ^{14}C and ^{36}Cl/Cl simultaneously with the same advective flow velocity in the range of 1 m/y. If one uses this flow velocity, the ^{4}He increase of $1 \cdot 10^{-9}$ cc/g per meter flow distance translates into a similar number of increase per year ($1 \cdot 10^{-9}$ cc/(g y)), neglecting the ascending water at Amusen, Dangarfield and Moorabinda. This would be an extremely high value. For comparison: in-situ production with U and Th concentrations in the range of (3.3±2.1) ppm U and (3.4±2.7) ppm Th respectively (Smith 2015) results in a helium production in groundwater of around $1 \cdot 10^{-12}$ cc/(g y) which is a factor of 1000 smaller. However, this high helium increase in the groundwater can be explained if one assumes that most of the helium is not from production within the aquifer but from the surrounding stagnant parts and from below (Torgersen and Clarke 1985; Torgersen and Ivey 1985; Torgersen and Clarke 1987). Exact details

of how this increase in Helium with time and flow distance can be explained will be targeted by the numerical modelling studies of this project.

Figure 3.13: Map of ^{14}C (top) and ^{36}Cl/Cl (bottom) in the Hutton Sandstone.

Figure 3.14: Map of ¹⁸O values (top) and ⁴He concentrations (bottom) in the Hutton Sandstone.
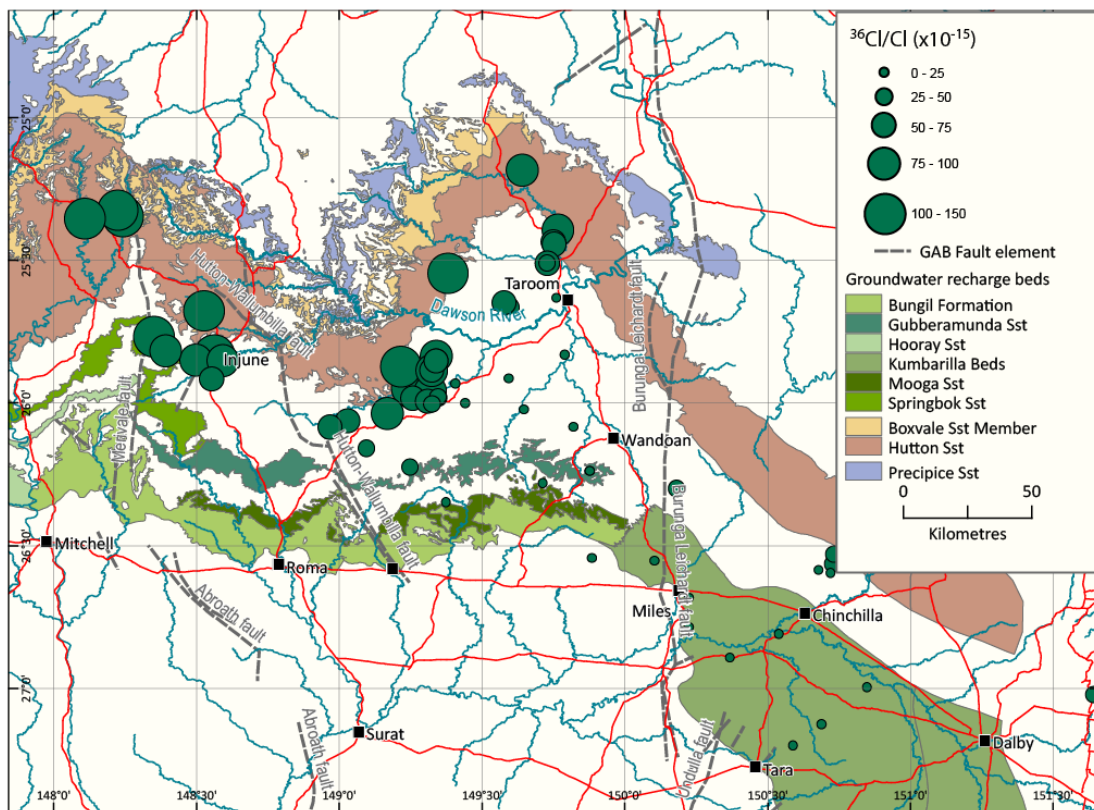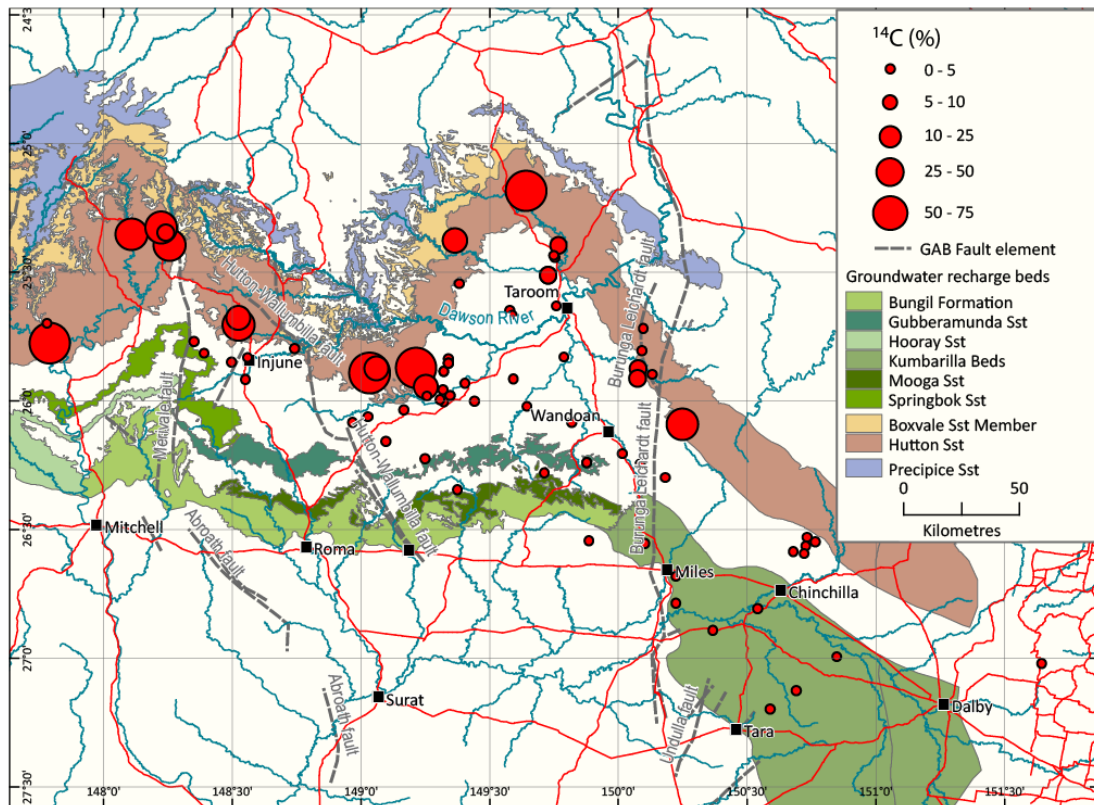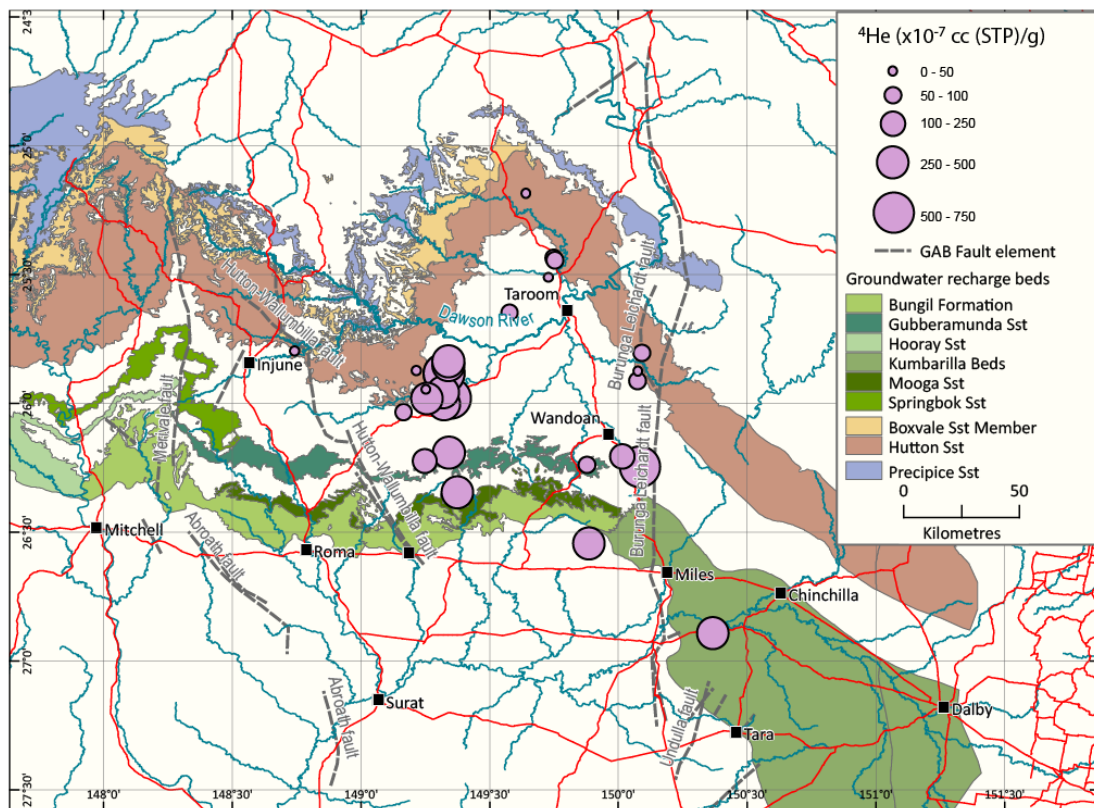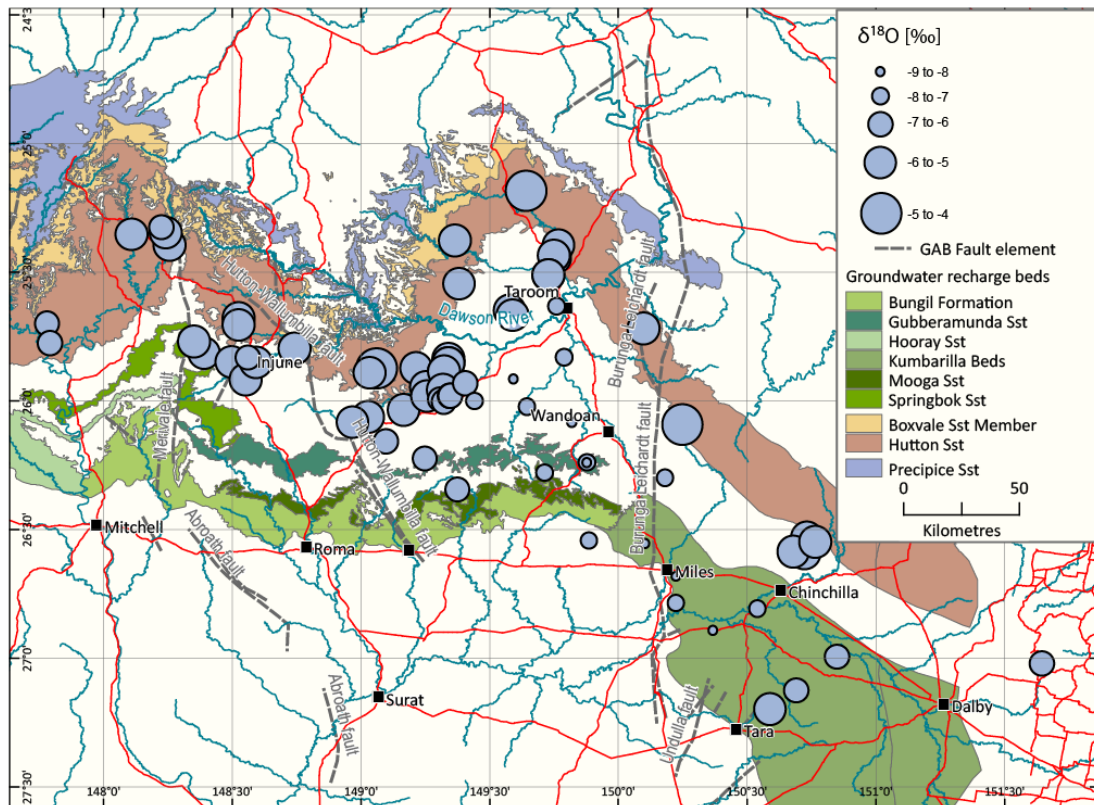
4 Discussion and conclusions

This multi-tracer investigation provided the first quantitative assessment of groundwater flow directions and velocities in the Precipice Sandstone aquifer. Combining several environmental tracer techniques into a consistent interpretation, it was possible to derive a first estimate of natural historical groundwater flow velocities prior to modern human influence and estimate recharge into the deeper Precipice Sandstone. Groundwater in the Precipice Sandstone is fresh over the whole area of the Mimosa syncline (mostly below 50mg/L chloride) and the tracer results indicate high flow velocities (0.8-1.5 m/y). In contrast to the findings in the Hutton Sandstone, the environmental tracers indicate a flow system that continues towards the south and shows no indication of discharge to the Dawson River.

- This study provided the first estimate to date for flow velocity in and recharge to the deeper Precipice Sandstone aquifer.
- Flow velocities in the Precipice are astonishingly high and indicate high recharge rates to this aquifer.
- The earlier findings for the Hutton Sandstone are confirmed by the new data.
- To constrain the water balance of the aquifer system as a whole, the connectivity *between* aquifers requires further investigation
- The combination of numerical modelling and tracer measurements is promising when targeting ^{14}C, $^{36}Cl/Cl$ and helium for calibration.
- Environmental tracer results reflect the natural flow system before human influence.

This study also increased the knowledge on the flow system of the Hutton Sandstone and confirmed earlier findings. Especially the recharge values in the range of 450ML/y obtained in the previous study are confirmed by the new data.

Several new insights into the hydrogeology of the Hutton Sandstone aquifer were obtained, including that it has more diverse flow paths than previously considered, a lower effective porosity and therefore transmissivity than earlier assumed, which results in higher vulnerability of the aquifer towards extraction. Whilst using environmental tracers to infer hydrogeological processes in GAB aquifers is not new, additional information was gained here by using a variety of tracers that can characterise the system at different spatial and temporal scales. In particular, the matching of age-dating tracers covering different timescales provided additional information. New insights are obtained about initial tracer concentrations at the beginning of the flow path and a preliminary quantification of the double porosity properties of the Hutton Sandstone. In the following, the Precipice Sandstone and Hutton Sandstone aquifer flow systems are reviewed and key recommendations to further characterise the Hutton and Precipice Sandstone aquifers are provided.

4.1   Precipice Sandstone flow system

Transects along the flow distance from the outcrop area towards the south were investigated for the tracers ^{18}O & ^{2}H, ^{14}C, $^{36}Cl/Cl$ and the noble gases He, Ne, Ar, Kr, Xe. The most convincing information of flow velocity came from ^{14}C because it appears to be best adapted to the time scale of groundwater flow in the Precipice. Distance velocities of 0.8 m/y to 2 m/y are in agreement with the decrease of ^{14}C with distance to the Precipice outcrop. $^{36}Cl/Cl$ stays more or less constant along the flow path and shows only indication of secular variations of $^{36}Cl/Cl$ ratios. These may be caused either by temporal changes in the ^{36}Cl production (that is: changes in cosmic radiation production of ^{36}Cl, due to e.g. variations in the Earth magnetic field) or by temporal changes in atmospheric chloride transport (that is: changes in the wind field or in proximity of the recharge area to the sea by sea-level changes during the last glaciation). Radioactive decay of the $^{36}Cl/Cl$

signal is not discernible in the transect of $^{36}Cl/Cl$ along flow distance, which confirms the high flow velocities derived from ^{14}C. The chemical parameters TDIC and chloride concentration stay relatively constant along the flow path and give confidence that the flow velocities derived from ^{14}C and $^{36}Cl/Cl$ are indeed reliable. The stable isotopes of water show no indication of variation due to palaeoclimate, in contrast to the earlier interpretation for the Hutton Sandstone (Suckow *et al.* 2016). Instead, they are more or less constant with flow distance. The heavy noble gases indicate infiltration temperatures between 15°C and 24°C, where the latter is in agreement with present mean annual soil temperatures in the area. Helium concentrations increase with flow distance and do so at a much higher rate than earlier observed in the literature of the GAB. This is probably due to the Precipice Sandstone aquifer being below the GAB aquifers and therefore receiving the first and more pronounced crustal helium flux from below.

In synthesis, the multi-tracer study in the Precipice Sandstone allowed the first estimate of deep recharge which gives values (as Darcy velocity) in the range of 110 mm/y to 315 mm/y. Together with estimates of the total cross-sectional area, derived from an estimate of the average thickness of Precipice Sandstone and the width of the cross-section through which the flow occurs, this results in a total intake of 1.1 GL/y to 6.6 GL/y for the Precipice Sandstone in the area of the Mimosa Syncline.

One has to keep in mind here, that this is the first quantitative recharge assessment for the Precipice Sandstone aquifer that we know of. These values have to be checked and confirmed by independent methods, like e.g. Chloride Mass Balance (CMB) or water level fluctuation. Since the Precipice Sandstone is not found outside of the Surat Basin (Ransley *et al.* 2015), the groundwater recharged to it needs to be fed into other aquifers, probably GAB aquifers.

4.2 Hutton Sandstone flow system

The new environmental tracer data further highlighted the complexity of the Hutton Sandstone flow system. As indicated earlier this system has several recharge areas, flow pathways and discharge zones. The new data confirms that waters south of the line Roma-Taroom are at the detection and dating limit of ^{14}C and $^{36}Cl/Cl$ and therefore cannot be assessed in terms of flow velocity and flow direction with the tracer methods applied so far. The stable isotope signature found in these waters earlier (Suckow *et al.* 2016) are confirmed, and re-interpreted in the light of the stable isotope data of the Precipice Sandstone, indicating that these waters are much older than the last glaciation (i.e. older than 17-20 ky). To shed light on the question how old these waters really are, one would need more exotic noble gas isotope measurements and specialized sampling methodologies in open bore holes. For the scope of the present study the main result is that these areas are not actively connected to the flow system of the Hutton Sandstone.

4.3 Tracers and numerical models

The present multi-tracer study provides at least three different environmental tracer targets for a calibration of a numerical flow and transport model in the Hutton Sandstone and Precipice Sandstone. First, ^{14}C can be traced throughout the Precipice as part of the calibration of a numerical groundwater flow and solute transport model. Second, in the Hutton Sandstone, a solute transport simulation would test the hypothesis of a rapid decrease of ^{14}C concentrations close to the recharge area and a decrease of $^{36}Cl/Cl$ along the flow path despite the comparably large flow velocity close to 1 m/y. This may require modelling the Hutton Sandstone with double porosity to match both tracers simultaneously. Third, a numerical description of flow and transport in the Precipice Sandstone would provide demonstration of the magnitude of flow velocities, and a testing of the tracer-based hypothesis of fast enough transport to have negligible radioactive decay for ^{36}Cl, but clearly measurable radioactive decay of ^{14}C.

Besides the obvious tracers ^{14}C and $^{36}Cl/Cl$, a numerical simulation can also target the concentrations measured for helium in groundwater. The advantage of this tracer is the much larger dynamic range as compared to ^{14}C and $^{36}Cl/Cl$. While the latter can be evaluated only over a concentration range of a factor of 100 (^{14}C) or 20 ($^{36}Cl/Cl$), helium concentrations in the aquifers under consideration vary by a factor of 5,000 and are therefore more sensitive to transport of old water into shallower aquifers and to diffusive

processes from the surrounding aquitards. These processes will be studied in detail in the last part of the present project.

References

Andrews, JN, Davis, S, Fabryka-Martin, J, Fontes, JC, Lehmann, BE, Loosli, HH, Michelot, J-L, Moser, H, Smith, B, Wolf, M (1989) The in-situ production of radioisotopes in rock matrices with particular reference to the Stripa granite. *Geochimica et Cosmochimica Acta* **53**, 1803–1815.

Andrews, JN, Lee, DJ (1979) Inert gases in groundwater from the Bunter Sandstone of England as indicators of age and palaeoclimatic trends. *Journal of Hydrology* **41**, 233-252.

APLNG (2014) Australia Pacific LNG Upstream 2013-2014 Groundwater Assessment Report. Available at http://www.aplng.com.au/pdf/Q-LNG01-75-RP-0001__Annual_GW__Report_Rev1_Final.pdf.

Ballentine, CJ, Burgess, R, Marty, B (2002) Tracing fluid origin, transport and interaction in the crust. In 'Noble Gases in Geochemistry and Cosmochemistry.' pp. 539-614.

Banks, EW, Smith, SD, Hatch, M, Burk, L, Suckow, A (2017) Sampling Dissolved Gases in Groundwater at in Situ Pressure: A Simple Method for Reducing Uncertainty in Hydrogeological Studies of Coal Seam Gas Exploration. *Environmental Science & Technology Letters* **4**, 535-539.

Barrows, TT, Stone, JO, Fifield, LK, Cresswell, RG (2002) The timing of the Last Glacial Maximum in Australia. *Quaternary Science Reviews* **21**, 159-173.

Bentley, HW, Phillips, FM, Davis, SN, Habermehl, MA, Airey, PL, Calf, GE, Elmore, D, Gove, HE, Torgersen, T (1986) Chlorine 36 Dating of Very Old Groundwater 1. The Great Artesian Basin, Australia. *Water Resources Research* **22**, 1991-2001.

Cook, PG, Böhlke, J-K (1999) Determining Timescales for Groundwater Flow and Solute Transport. In 'Environmental Tracers in Subsurface Hydrology.' (Eds PG Cook, AL Herczeg.) pp. 1-30. (Kluwer Academic Press: Boston, Mass.)

Craig, H (1961) Isotopic variations in meteoric waters. *Science* **133**, 1702-1703.

DNRM, 2013. Queensland Department of Natural Resources and Mines groundwater database. Queensland Department of Natural Resources and Mines,

Einstein, A (1905) Über die von der molekularkinetischen Theorie der Wärme geforderte Bewegung von in ruhenden Flüssigkeiten suspendierten Teilchen. *Annalen der Physik* **17**, 549-560.

Esteban, L, Pervukhina, M, Mallants, D, Clennell, B, Verrall, M, Raven, M, Nguyen, D (2015) Experimental Study of Background Permeability of Formations in the Walloon Sub Group (Surat Basin). CSIRO.

Gonfiantini, R (1986) Environmental Isotopes in Lake Studies. In 'Handbook of Environmental Isotope Geochemistry. Vol. 2, The Terrestrial Environment B.' (Eds P Fritz, J-C Fontes.) Vol. 2 pp. 113-168.

Habermehl, MA (1980) The Great Artesian Basin, Australia. *BMR Journal of Australian Geology & Geophysics* **5**, 9-38.

Habermehl, MA, Devonshire, J, Magee, JW (2009) Sustainable groundwater allocations in the intake beds of the Great Artesian Basin in New South Wales: Final report. Bureau of Rural Sciences, Canberra.

Heaton, THE, Vogel, JC (1981) "Excess Air" in Groundwater. *Journal of Hydrology* **50**, 201-216.

Hodgkinson, J, Hortle, A, McKillop, M (2010) The Application of Hydrodynamic Analysis in the Assessment of Regional Aquifers for Carbon Geostorage: Preliminary Results for the Surat Basin, Queensland. *APPEA Journal* 1-18.

Hoffmann, G, Jouzel, J, Masson, V (2000) Stable water isotopes in atmospheric general circulation models. *Hydrological Processes* **14**, 1385-1406.

IAEA (2013) 'Isotope Methods for Dating Old Groundwater.' (International Atomic Energy Agency: Vienna)

IAEA/WMO (2015) Global Network for Isotopes in Precipitation. The GNIP Database. Release 3, October 1999.

Jähne, B, Heinz, G, Dietrich, W (1987) Measurement of the diffusion coefficients of sparingly soluble gases in water. *Journal of Geophysical Research: Oceans* **92**, 10767-10776.

King, DB, Saltzman, ES (1995) Measurement of the diffusion coefficient of sulfur hexafluoride in water. *Journal of Geophysical Research: Oceans* **100**, 7083-7088.

Königer, P, Leibundgut, C, Link, T, Marshall, JD (2010) Stable isotopes applied as water tracers in column and field studies. *Organic Geochemistry* **41**, 31-40.

Königer, P, Leibundgut, C, Stichler, W (2009) Spatial and temporal characterisation of stable isotopes in river water as indicators of groundwater contribution and confirmation of modelling results; a study of the Weser river, Germany. *Isotopes in Environmental and Health Studies* **45**, 289 - 302.

Lamontagne, S, Taylor, AR, Batlle-Aguilar, J, Suckow, A, Cook, PG, Smith, SD, Morgenstern, U, Stewart, MK (2015) River infiltration to a subtropical alluvial aquifer inferred using multiple environmental tracers. *Water Resources Research* n/a-n/a.

Maloszewski, P, Zuber, A (1985) On the theory of tracer experiments in fissured rocks with a porous matrix. *Journal of Hydrology* **79**, 333-358.

Mook, WG, Plicht, Jvd (1999) Reporting 14C activities and concentrations. *Radiocarbon* **41**, 227-239.

OGIA, D (2016) Underground Water Impact Report for the Surat Cumulative Management Area. Department of Natural Resources and Mines, Office of Groundwater Impact Assessment, Brisbane.

Phillips, FM (2013) Chlorine-36 dating of old groundwater. In 'Isotope Methods for Dating Old Groundwater.' (Eds A Suckow, PK Aggarwal, LJ Araguas-Araguas.) pp. 125-152. (International Atomic Energy Agency: Vienna)

Plummer, LN, Glynn, PD (2013) Radiocarbon Dating in Groundwater Systems. In 'Isotope Methods for Dating Old Groundwater.' (Eds A Suckow, PK Aggarwal, LJ Araguas-Araguas.) pp. 33-89. (International Atomic Energy Agency: Vienna)

Pollock, DW (1994) User's guide for MODPATH/MODPATH-PLOT, Version 3: A particle post-processing package for MODFLOW, the U. S. Geological Survey finite-difference ground-water flow model. U. S. Geological Survey.

Purtschert, R, Yokochi, R, Sturchio, NC (2013) 81Kr dating of old groundwater. In 'Isotope Methods for Dating Old Groundwater.' (Eds A Suckow, PK Aggarwal, LJ Araguas-Araguas.) pp. 91-124. (International Atomic Energy Agency: Vienna)

Radke, BM, Ferguson, J, Cresswell, RG, T.R., R, Habermehl, MA (2000) 'Hydrochemistry and implied hydrodynamics of the Cada-owie-Hooray Aquifer Great Artesian Basin.' (Bureau of Rural Sciences, Australia:

Raiber, M, Suckow, A (2017) Hydrochemical assessment of the Hutton and Precipice sandstones in the northern Surat Basin. CSIRO, Australia, CSIRO, Australia. Available at https://gisera.org.au/wp-content/uploads/2015/11/Water-6-Report-Milestone-3.1-JUNE-2017.pdf.

Ransley, TR, Radke, BM, Feitz, AJ, Kellett, JR, Owens, R, Bell, J, Stewart, G, Carey, H, 2015. Hydrogeological Atlas of the Great Artesian Basin.. 1 ed. Scale 1:10000000. Geoscience Australia, Canberra, `.

Ransley, TR, Smerdon, BDe (2012) Hydrostratigraphy, hydrogeology and system conceptualisation of the Great Artesian Basin. CSIRO Water for a Healthy Country Flagship, Australia.

Reading, L, McIntyre, N, Larsen, J, Bulovic, N, Jarihani, A, Dinh, L, Finch, W (2016) Recharge Estimation in the Surat Basin. Final Report. The University of Queensland, Brisbane.

Rozanski, K (1985) Deuterium and Oxygen-18 in European groundwaters - Links to atmospheric circulation in the past. *Chemical Geology (Isotope Geoscience Section)* **52**, 349-363.

Smerdon, BD, Davies, PJ (2012) Regional water budget. In 'Water resource assessment for the Surat region. A report to the Australian Government from the CSIRO Great Artesian Basin Water Resource Assessment.' pp. 111-116. (CSIRO Water for a Healthy Country Flagship, Australia.:

Smerdon, BD, Ransley, TRe (2012) Water resource assessment for the Surat region. CSIRO Water for a Healthy Country Flagship, Australia.

Smith, SD (2015) Geochemical baseline monitoring: quartz-helium trial. CSIRO, Adelaide.

Solomon, DK, Cook, PG, Plummer, LN (2006) Models of Groundwater Ages and Residence Times. In 'Use of Chlorofluorocarbons in Hydrology. A Guidebook.' pp. 73-88. (International Atomic Energy Agency (IAEA): Vienna)

Sonntag, C, Schoch-Fischer, H (1985) Deuterium and Oxygen 18 in Water Vapour and Precipitation: Application to Atmospheric Water Vapour Transport and to Paleoclimate. *Isotopenpraxis* **21**, 193-198.

Stuiver, M, Polach, HA (1977) Discussion of Reporting of 14C Data. *Radiocarbon* **19**, 355-363.

Stute, M, Forster, M, Frischkorn, H, Serejo, A, Clark, JF, Schlosser, P, Broecker, WS, Bonani, G (1995) Cooling of Tropical Brazil (5°C) During the Last Glacial Maximum. *Science* **269**, 379-383.

Stute, M, Talma, S (1997) Glacial temperatures and moisture transport regimes reconstructed from noble gases and d18O, Stampriet aquifer, Namibia.

Suckow, A (2009) Chapter 9 Analysis of Radionuclides. In 'Radioactivity in the Environment.' (Ed. F Klaus.) Vol. Volume 16 pp. 363-406. (Elsevier:

Suckow, A (2012) 'Lumpy - an interactive Lumped Parameter Modeling code based on MS Access and MS Excel., EGU 12.' Vienna. (European Geosciences Union. Available at http://meetingorganizer.copernicus.org/EGU2012/EGU2012-2763.pdf

Suckow, A (2013) System Analysis using Multi-Tracer Approaches. In 'Isotope Methods for Dating Old Groundwater.' (Eds A Suckow, PK Aggarwal, LJ Araguas-Araguas.) pp. 217-244. (International Atomic Energy Agency: Vienna)

Suckow, A (2014) The age of groundwater – Definitions, models and why we do not need this term. *Applied Geochemistry* **50**, 222-230.

Suckow, A, Dumke, I (2001) A database system for geochemical, isotope hydrological, and geochronological laboratories. *Radiocarbon* **43**, 325-337.

Suckow, A, Taylor, AR, Davies, P, Leaney, FW (2016) Geochemical Baseline Monitoring. Final Report. CSIRO, Australia. Available at https://gisera.org.au/wp-content/uploads/2012/06/Project-4-Geochemical-Baseline-Report-201602.pdf.

Sudicky, EA, Frind, EO (1981) Carbon 14 dating of groundwater in confined aquifers: Implications of aquitard diffusion. *Water Resources Research* **17**, 1060-1064.

Tadros, CV, Hughes, CE, Crawford, J, Hollins, SE, Chisari, R (2014) Tritium in Australian precipitation: A 50 year record. *Journal of Hydrology* **513**, 262-273.

Taylor, AR, Pichler, MM, Olifent, V, Thompson, J, Bestland, EA, Davies, PJ, Lamontagne, S, Suckow, AO, Robinson, NI, Love, A (2015) Groundwater Flow Systems of North Eastern Eyre Peninsula: a multi-disciplinary approach: hydrogeology, geophysics and environmental tracers. Facilitating Long Term Outback Water Solutions —Stage 2. Goyder Institute for Water Research.

Torgersen, T, Clarke, WB (1985) Helium accumulation in groundwater, I: An evaluation of sources and the continental flux of crustal 4He in the Great Artesian Basin, Australia. *Geochimica et Cosmochimica Acta* **49**, 1211-1218.

Torgersen, T, Clarke, WB (1987) Helium accumulation in groundwater, III. Limits on helium transfer across the mantle-crust boundary beneath Australia and the magnitude of mantle degassing. *Earth and Planetary Science Letters* **84**, 345-355.

Torgersen, T, Ivey, GN (1985) Helium accumulation in groundwater. II: A model for the accumulation of the crustal 4He degassing flux. *Geochimica et Cosmochimica Acta* **49**, 2445-2452.

Torgersen, T, Purtschert, R, Phillips, FM, Plummer, LN, Sanford, W, Suckow, A (2013) Defining Groundwater Age. In 'Isotope Methods for Dating Old Groundwater.' (Eds A Suckow, PK Aggarwal, LJ Araguas-Araguas.) pp. 21-32. (International Atomic Energy Agency: Vienna)

Torgersen, T, Stute, M (2013) Helium (and other Noble Gases) as a Tool for Understanding Long Timescale Groundwater Transport. In 'Isotope Methods for Dating Old Groundwater.' (Eds A Suckow, PK Aggarwal, LJ Araguas-Araguas.) pp. 179-216. (International Atomic Energy Agency: Vienna)

Visser, A, Broers, HP, Bierkens, MFP (2007) Dating Degassed Groundwater with 3H/3He. *Water Resourources Research* **43**,

Visser, A, Schaap, JD, Broers, HP, Bierkens, MFP (2009) Degassing of 3H/3He, CFCs and SF6 by denitrification: Measurements and two-phase transport simulations. *Journal of Contaminant Hydrology* **103**, 206-218.

Vogel, JC (1967) Investigation of groundwater flow with radiocarbon. In 'Isotopes in Hydrology. Vienna'. pp. 255-368. Vienna)

Weiss, RF (1968) Piggyback samplers for dissolved gas studies on sealed water samples. *Deep Sea Research* **15**, 659-699.

Appendix A

A.1 Using environmental tracers to quantify groundwater time scales

Using environmental tracers as age indicators relies on time-dependent concentrations of trace substances in water. The trace substances have a known time-dependent input function as indicated on the left of Figure A.1. Tracers can be stable and conservative, like for example ^{18}O and ^{2}H, CFCs and SF_6. Other trace substances can be radioactive, and in this case the natural radioactivity can provide time information also when the input function at recharge is constant, as for example, with ^{14}C and ^{36}Cl. Also, a combination of time-dependent input and radioactive decay is possible such as with ^{3}H and ^{85}Kr, as long as the time-dependent input is quantified. Or, the concentration of the tracer can increase with time along the flow path, e.g. due to underground production, as is the case with ^{4}He. Any age deduced from the measured concentration of an environmental tracer, however, is never unique, no matter what tracer is used. Figure A.1 illustrates this.
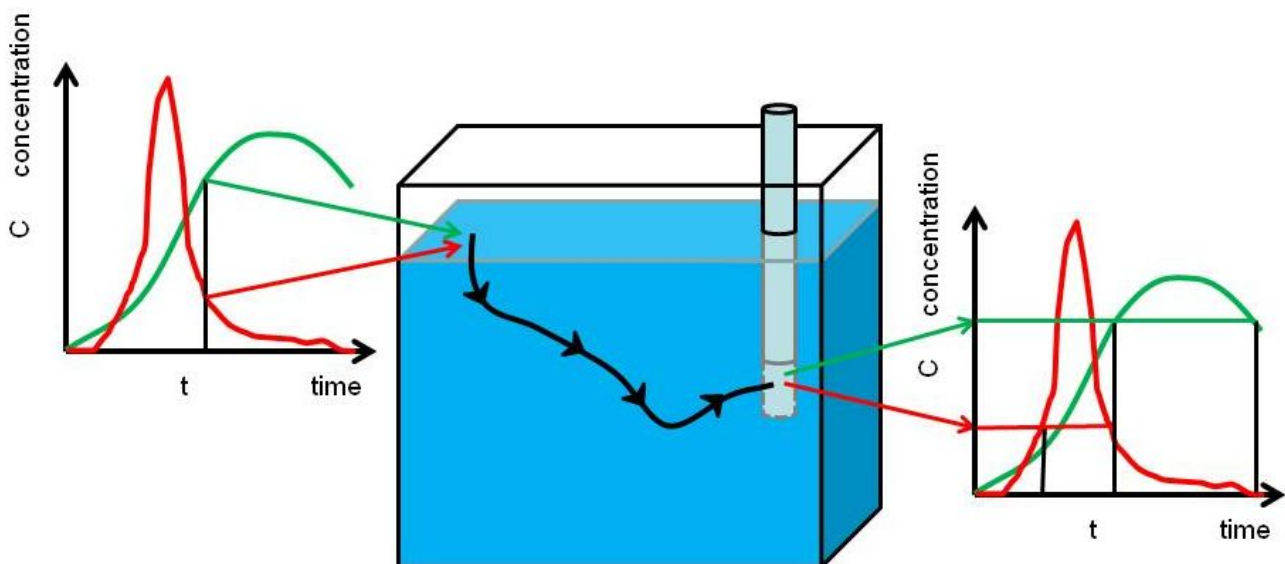
Figure A.1: Principle of the application of environmental tracers to deduce groundwater age (Suckow 2014)

The tracer concentration always needs to be known at the recharge site ("input function", represented by the red and green curve on the left, indicating two different tracers). However, the measured concentration at the well screen allows for several moments in time to be deduced (horizontal red and green lines on the right, each giving two ages, represented as vertical black lines). Therefore every application needs a combination of several tracers to derive a unique value on the time axis (middle black line agreeing both to the red and green concentrations on the input curve). Details of different age definitions and how they relate to common conceptions of human age can be found in Suckow (2014). Only those tracer properties will be discussed in the following sections that are important in the context of the present project. It is, however, important to note that all tracer methods determine the distance velocity v within the aquifer (unit: m/year). This is related to the Darcy velocity q (volumetric groundwater flux in cubic meters per square meter aquifer cross section and year; also expressible as m/y) by the (effective) porosity n_e via $v=q/n_e$. Tracer derived velocities are therefore always larger than Darcy velocities and the factor n_e between v and q needs an independent assessment.

A.2   Tracers used

Tracers used in this report to interpret flow velocities were the stable isotopes of water (^{18}O and ^{2}H), CFCs, SF$_6$, tritium (^{3}H), ^{14}C, ^{36}Cl and ^{4}He. They will be introduced shortly in the following sections. The chemical compounds CFCs and SF$_6$ are of anthropogenic origin, are dissolved in water and recharge times can be deduced from their known atmospheric concentration. The other tracers are radioactive (^{14}C, ^{36}Cl, ^{3}H) or stable isotopes (^{2}H, ^{18}O, ^{4}He) of elements. Isotopes (from the Greek word 'iso topos' for 'same place' – meaning the same place in the periodic table of the elements) are varieties of atoms of one element with identical chemical behaviour (since they belong to the same element) but slightly different mass, which can result in fractionation during physical or biological processes. This difference in mass is due to different number of neutrons. Since the chemical properties are determined by the number of electrons in the hull, which in a neutral atom equals the number of protons in the nucleus, all isotopes show the same chemical behaviour of the element. This makes isotopes ideal tracers. Too few or too many neutrons relative to protons renders a core unstable, which is why some isotopes are radioactive. Environmental tracers use all these properties to investigate natural processes – known concentration at the time of recharge, identical chemical behaviour since it is the same element, differences in mass that lead to fractionation, and radioactive decay that provides a natural 'clock' for natural processes.

A.2.1 STABLE ISOTOPES OF WATER

The water molecule H$_2$O is formed of the elements hydrogen and oxygen. While the most abundant isotopes of hydrogen and oxygen are ^{1}H and ^{16}O, respectively (forming ^{1}H$_2$^{16}O), both elements have a stable and rare isotope, ^{2}H and ^{18}O. In the natural water cycle these isotopes behave as normal water. In fact they *are* water, forming molecules with slightly different masses (e.g. ^{2}H^{1}H^{16}O and ^{1}H$_2$^{18}O). Nevertheless, the different isotopic species of water are slightly enriched during different natural processes, the most important being phase transitions (e.g. from liquid to gas phase). The heavier molecules, containing ^{2}H and ^{18}O, are slightly enriched (by a few ‰ only) in the less mobile phase. For example, the ocean will contain slightly more ^{2}H and ^{18}O per gram water than the water vapour formed from it, and the raindrop will contain slightly more ^{2}H and ^{18}O than the cloud it formed from. The magnitude of this isotopic difference depends on the temperature prevailing during the phase transition (evaporation or condensation). These slight differences in the isotopic ratio R are expressed as per mil deviation of a standard, called SMOW (Standard Mean Ocean Water) using the delta notation:

$$\delta \equiv \frac{R_{Sample} - R_{Standard}}{R_{Standard}} = \frac{R_{Sample}}{R_{Standard}} - 1 \quad [\cdot 1000‰] \tag{2}$$

Since the standard is ocean water and since, as mentioned, the water vapour derived from it will have less of the heavy isotopic species, and since nearly the entire global water cycle happens after this phase transition, most isotopic values for δ^{18}O and δ^{2}H in water samples are negative. One has to keep in mind that the fractionation effects in stable isotopes are very small, per mil only, whereas the effects of radioactivity (^{3}H, ^{14}C, ^{36}Cl) or concentration (CFCs, SF$_6$) are comparably large: several percent or a factor of two to ten. As a consequence of natural isotopic enrichment processes, several effects can be observed.

Continental effect

Air masses losing water as rain when moving inland will gradually deplete in the heavy isotopes. This means that rain falling further inland will be more negative in δ^{18}O and δ^{2}H than close to the coast. The effect was first described for Europe (Sonntag and Schoch-Fischer 1985) and later verified all over the world, see http://www-naweb.iaea.org/napc/ih/documents/userupdate/Waterloo/. The magnitude of this effect is on the order of 0.2‰/100 km in δ^{18}O. For the study here the effect is unimportant, because the size of the whole study area is not much more than 100 km and the typical measurement precision for δ^{18}O is 0.1‰.

Evaporation effect

If a water body evaporates, the water vapour will be isotopically lighter (more negative in δ values) than the remaining water body. As a consequence, the remaining water body will gradually develop more positive values in $\delta^{18}O$ and $\delta^{2}H$. This is a useful tool in water balance investigations of lake studies (Gonfiantini 1986) and allows determining the evaporated fraction of lakes, channels and rivers. Evaporation can be easily determined in a plot of $\delta^{2}H$ versus $\delta^{18}O$ because the slope of evaporating waters in this plot is characteristically smaller – around 4 to 6 – than the global meteoric water line GWML (Craig 1961) on which most other precipitation and groundwater values are situated and which has a slope of 8. The slope of the evaporation line depends on relative humidity, for tropical conditions with 100% relative humidity it approaches the slope of 8 of the GMWL. For the present study the evaporative effect is only important in case groundwater infiltrates from rivers, which is not to be expected.

Temperature effect

The isotopic fractionation is temperature dependent, and at lower temperatures the heavy species will be even less mobile than at higher temperatures. Therefore rain in winter will have a hydrogen and oxygen isotopic composition slightly lighter (less heavy isotopes, more negative delta values) than in summer. The magnitude of this effect is 0.5‰/°C in $\delta^{18}O$ as global average but can vary considerably on a local scale. This seasonal effect is most pronounced in precipitation itself and meanwhile used to calibrate General Circulation Models (GCM) of the atmosphere (Hoffmann *et al.* 2000). The seasonal temperature effect in stable isotopes is also discernible in the runoff signal in rivers (Königer *et al.* 2009), and in the soil zone (Königer *et al.* 2010). In groundwater this seasonal signal in stable isotopes is only discernible for very young groundwater (typically <4years), which makes this seasonality a useful tool in Karst systems.

Another temperature effect is more important when studying old groundwater; Pleistocene precipitation was recharging groundwater under colder conditions than today and these colder temperatures are reflected by isotope values that are typically 20‰ more negative in $\delta^{2}H$ for Pleistocene palaeowaters than for modern waters in Europe (Rozanski 1985). This corresponds to ≈2.5‰ more negative values in $\delta^{18}O$ for Pleistocene palaeowaters. The reason for this variation between the last glaciations and today is, however, not only due to temperature. Since during the last glaciations 3% of the global water volume was stored in the ice caps and since this ice-stored water was depleted in ^{18}O and ^{2}H (had more negative isotope values) the remaining ocean water was roughly 1.2‰ more positive than today. The actual temperature effect in Europe therefore corresponds to 3.7‰ in ^{18}O. The global effect will vary from place to place and only few palaeoclimate records exist on the southern hemisphere (Stute *et al.* 1995; Stute and Talma 1997). Some of these show positive and some negative shifts in ^{18}O values during the last ice-age, with no reliable record published to date for Australia. In any case, stable isotope measurements may allow discerning water recharged 10 ky ago from those recharged today. This is a useful application to confirm other tracers, like ^{14}C and ^{36}Cl, used to derive flow velocities.

A.2.2 ANTHROPOGENIC DECADAL TRANSIENT TRACERS (^{3}H, CFCS, SF$_6$)

The transient tracers of anthropogenic origin can be used for timescales of years to a few decades. These comprise ^{3}H, CFCs and SF$_6$ and are called transient because their input concentration changes with time.

Tritium

Tritium (^{3}H) is the radioactive isotope of hydrogen and as such is part of the water molecule. Tritium is commonly measured in Tritium Units (TU), where one tritium unit corresponds to a ratio of ^{3}H to normal hydrogen of 10^{-18}, or to a tritium related specific radioactivity of 0.119 Bq per kg water. The ^{3}H presently observed predominantly in shallow groundwater is largely a result of atmospheric hydrogen bomb tests carried out in the sixties. Natural background of tritium in Australia is below 5 TU. Figure A.1 shows the time series of ^{3}H content in precipitation in Kaitoke, New Zealand, where the longest record on the southern hemisphere is available. For comparison, this record is displayed together with some stations in Australia (IAEA/WMO 2015). Evidently, the tritium fallout in precipitation in Australian stations was slightly

higher around the bomb era than it was in New Zealand, which is due to a higher continental effect in Australia equivalent to higher dilution of the tritium input by oceanic (tritium-free) moisture in New Zealand. While the highest measurement in NZ was 76 TU in September 1966, some results in Adelaide, Melbourne, Brisbane and Alice Springs have values between 100 and 300 TU until 1972, which corresponds to the last French nuclear tests in the 100kt range in Mururoa. Unfortunately, while there is a recent evaluation of ^{3}H data in precipitation (Tadros *et al.* 2014), these contain no numerical values and have not been uploaded to the GNIP record as of August 2015 (IAEA/WMO 2015). Therefore, no Australian values are available for precipitation later than 1990.

Since ^{3}H is radioactive, Figure A.2 also displays how radioactive decay from some dates onward decreases the ^{3}H signal (blue lines). These lines give evidence that tritium alone cannot distinguish different recharge years uniquely, since rain from many different rainfall events would have 3-6 TU today. Therefore, although ^{3}H is radioactive, the way to use it as a groundwater tracer is largely like a dye, that is like CFCs and SF$_6$ are used, and hardly as a radioactive substance, as is the case for ^{14}C and ^{36}Cl (see below). A groundwater sample containing ^{3}H of more than 0.2 TU is an indication that part of the water recharged later than 1963, which corresponds to the peak in ^{3}H in precipitation in Figure A.2. *How much* of such young water is in the sample or *when* it was infiltrated cannot be uniquely quantified from one tritium measurement alone.
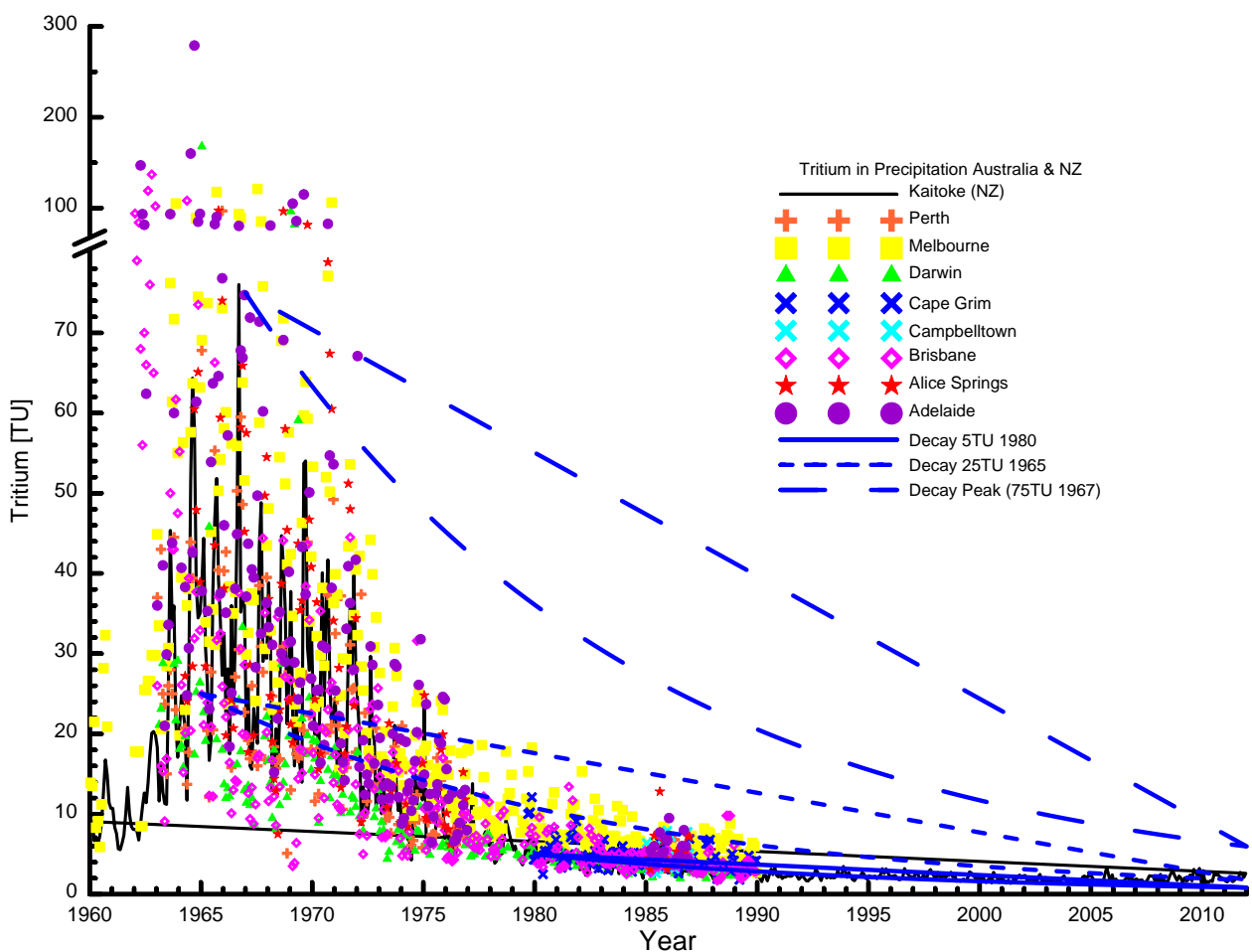
Figure A.2: Input function of tritium in Kaitoke and several Australian stations (IAEA/WMO 2015)

A.2.3 RADIOACTIVE TRACERS FOR OLD WATER (^{14}C, ^{36}CL)

Radioactive tracers used for the longer timescales are ^{14}C and ^{36}Cl. Both are cosmogenic nuclides, naturally produced in the upper atmosphere from cosmic radiation. For radioactive tracers with known or constant input function, an apparent age can be derived from concentrations using the equation of radioactive decay:

$$C(t) = C_0 \exp(-\lambda t) \Leftrightarrow t = \frac{1}{\lambda} \ln\left(\frac{C_0}{C(t)}\right) \tag{3}$$

Here t is the apparent age (Suckow 2014), λ is the decay constant, corresponding to $\ln(2)/t_{1/2}$ and $t_{1/2}$ is the half-life. $C(t)$ is the measured concentration in the sample and C_0 the concentration at recharge. For most groundwater tracers C_0 is insufficiently known *a priori* and needs to be determined in the recharge area. Such an empirical determination involves a cross-plot with a tracer for the next younger timescale (Suckow 2013). For ^{14}C this may be ^3H, CFCs, SF_6 and ^{85}Kr. For the initial value of $^{36}Cl/Cl$, ^{14}C can be favourably used as this young tracer. For ^{14}C in combination with CFCs or ^3H, input functions for both tracers can be compared with measured values on a dual tracer plot and a constant factor to the atmospheric ^{14}C ratio can be fitted, as successfully demonstrated in Lamontagne *et al.* (2015) or Taylor *et al.* (2015). For $^{36}Cl/Cl$ the initial value would be obtained from those samples that still contain radiocarbon, if mixtures between water of different age can be excluded. Typical applications allow the determination of timescales up to five half-lives, so how far a tracer can be used into the past strongly depends on the kind of tracer.

Radiocarbon

Radiocarbon or ^{14}C is probably the most used tracer for 'dating' groundwater in Australia. Radiocarbon has a half-life of 5730 years, which allows determining flow velocities and constraining timescales between some thousand and approximately 30,000 years. For ^{14}C, the actually measured value is not the absolute concentration of ^{14}C in water, but the isotopic ratio of $^{14}C/^{12}C$ in the Total Dissolved Inorganic Carbon (TDIC), which is the sum of dissolved CO_2, HCO_3^- and CO_3^{2-}. The unit for this ratio of $^{14}C/^{12}C$ was pMC (percent Modern Carbon, (Stuiver and Polach 1977)) or more recently %, where 100% corresponds to the atmospheric $^{14}C/^{12}C$ ratio in 1950 (Mook and Plicht 1999). The basic assumption is that the isotopic ratio of $^{14}C/^{12}C$ changes only by radioactive decay of ^{14}C. Radiocarbon can be measured very precisely (better 0.1%) and with a very low detection limit of less than 0.1% via Accelerator Mass Spectrometry (AMS). In practical groundwater studies, especially in deep aquifers, a few % of ^{14}C should be considered as practical detection limit, since leaky casings or small hydraulic connections in the bore annulus can never completely be excluded.

Very often however, radioactive decay is not the only process decreasing ^{14}C in groundwater. All geochemical changes increasing TDIC or alkalinity can potentially decrease $^{14}C/^{12}C$ (Plummer and Glynn 2013). This is of special importance when fossil sources of carbon are available, as is obviously the case in the coal seam gas districts. Also for the GAB as a whole, an increase in alkalinity (and hence TDIC) is known with flow distance (Radke *et al.* 2000; Ransley and Smerdon 2012). A possibility to avoid this geochemical influence, which causes the water samples to look 'too old', is to consider only the concentration of ^{14}C (e.g. as ^{14}C atoms per litre water), in analogy to general practice for ^{36}Cl (see below). This case is easier than ^{36}Cl, because underground production of ^{14}C is negligible and therefore most underground sources of carbon can be considered ^{14}C-free and would not influence the ^{14}C concentration. If N_A is the Avogadro constant, TDIC is expressed as mmol/L carbon, $^{14}C/^{12}C$ in % and ^{14}C as atoms/L, then the recalculation of % into atoms/L ^{14}C is:

$$^{14}C[atoms/L] = \frac{^{14}C}{^{12}C}[\%] \frac{1}{100} \frac{TDIC}{1000} N_A 1.175 \cdot 10^{-12} \tag{4}$$

The number $1.175 \cdot 10^{-12}$ corresponds to the isotope ratio $^{14}C/^{12}C$ of modern carbon, which can be calculated from the specific activity of 0.226 Bq/gC and its physical half-life of 5730 years (Mook and Plicht 1999).

There are many geochemical 'correction' models which are all designed to derive the initial 'no decay' concentration C_0 for Equation 3. Since they will not be applied in this report they are not discussed in detail, and the interested reader is referred to the detailed description by Plummer and Glynn (2013).

Chlorine-36

The application of ^{36}Cl is very analogous to ^{14}C and the basic idea also follows Equation 3, with the important difference that the half-life of ^{36}Cl is much longer ($301,000\pm4,000$ years) (Phillips 2013). The

applicable time range therefore is between 50,000 and approximately one million years. This means [36]Cl behaves in comparison to ^{14}C similarly as ^{14}C behaves in comparison to [3]H. Also in the case of [36]Cl, the actually measured value is the isotopic ratio of [36]Cl/Cl. A general complication of [36]Cl is that it is produced in the subsurface (Andrews *et al.* 1989), mainly by neutron capture of [35]Cl and to a much smaller extent of potassium-39 ([39]K). The thermal neutrons in both cases come from uranium (U) and thorium (Th) in the aquifer. As a result of this underground production, the [36]Cl/Cl ratio normally does not approach zero but a non-zero value that has to be determined empirically in each aquifer. Chloride (Cl) as the carrier for the dating isotope has the advantage of being a much more conservative substance in groundwater than TDIC is for [14]C. Nevertheless, already in the first applications in the GAB the basic problems of dilution with 'dead' Cl and underground production of [36]Cl were discussed (Bentley *et al.* 1986). The Cl concentration along the flow path is necessary information for the interpretation of [36]Cl, as is the knowledge of the final value, to which the [36]Cl/Cl ratio develops for groundwater being much older than the dating range of [36]Cl. Data interpretation typically involves a discussion of plots of [36]Cl/Cl versus Cl concentration, [36]Cl/Cl versus [36]Cl concentration and [36]Cl concentration versus Cl concentration, as discussed in detail by Phillips (2013). In this book chapter, also a sufficiently general model of [36]Cl evolution in groundwater is described, which will be summarized next.

The Phillips Model for [36]Cl

In Chapter 6 of IAEA (2013) Fred M. Phillips described an easy mass balance equation for the absolute [36]Cl concentration in an aquifer. The model incorporates radioactive decay of the recharged [36]Cl, underground production in the aquifer towards a secular equilibrium ratio of [36]Cl/Cl and an additional source of chloride, like e.g. diffusion from an adjacent aquitard, which may have another [36]Cl/Cl ratio in secular equilibrium. The formula for the [36]Cl evolution with time is:

$$^{36}\text{Cl}(t) = R_m \text{Cl}_m = R_r \text{Cl}_r \exp(-\lambda t) + \left[R_1 \text{Cl}_r + \frac{F_{\text{Cl}}}{\lambda}(R_2 - R_1) \right] \left(1 - \exp(-\lambda t) \right) + R_2 F_{\text{Cl}} t \quad (5)$$

In this formula $^{36}\text{Cl}(t)$ is the absolute [36]Cl concentration [atoms/L], which corresponds to the measured [36]Cl/Cl ratio (R_m) multiplied with the measured chloride concentration Cl_m [atoms/L]. Further R_r, R_1 and R_2 are the isotopic ratios of [36]Cl/Cl in the recharge area (r), in secular equilibrium in the aquifer (*1*) and the adjacent aquitard (*2*) respectively. F_{Cl} is the flux of chloride from the aquitard to the aquifer [atoms/(L·year)], and λ is the decay constant of [36]Cl.

The model is general enough, that it can be applied to radiocarbon as well. In this case R_1 and R_2 are both zero, since no underground production takes place for ^{14}C, and it describes the dilution of the (measured) ^{14}C/C ratio with 'dead' TDIC. In any case it is necessary to support the findings from ^{14}C and [36]Cl with other tracers such as helium.

A.2.4 HELIUM AS A TRACER

The helium isotope [4]He is produced in the underground from the U/Th decay chains since these two elements are abundantly present at ppm concentration level in the rock matrix. Every alpha particle from the decay chains contributes a [4]He atom and most of these are released to the groundwater and pore water (Torgersen and Stute 2013). Figure A.3 displays the decay chain of [238]U (Suckow 2009) and each yellow arrow in it represents an alpha particle, corresponding to the creation of a helium atom. One atom of [238]U therefore will produce a total of eight [4]He atoms when decaying to [206]Pb.

The easiest, but seldom fulfilled assumption is that [4]He in groundwater increases constantly with time according to the formula (Andrews and Lee 1979):

$$\frac{dc(^4\text{He})}{dt} = \frac{\rho_R}{\rho_W} \Lambda \frac{1 - n_{tot}}{n_{eff}} (1.19 \cdot 10^{-13}[\text{U}] + 2.88 \cdot 10^{-14}[\text{Th}]) \quad (6)$$

Here $c(^4\text{He})$ is the measured concentration of [4]He in groundwater and $dc(^4\text{He})/dt$ is its increase per year in [cc(STP)/(g·year)]. ρ_R and ρ_W are the rock and water densities, Λ is a release factor of helium from the rock

which empirically is always 1, and n_{tot} and n_{eff} are the total and effective porosities valid for the groundwater flow. Uranium [U] and thorium [Th] concentrations in this formula are given as ppm. Typical uranium and thorium concentrations in aquifer rocks are in the range of fractions of a ppm to several ppm resulting in typical production rates of $1 \cdot 10^{-13}$ to $5 \cdot 10^{-11}$ cc(STP)/(g·year). Values for the Hutton and Precipice Sandstones in the Surat basin range from 3–6 ppm and 3–8 ppm for U and Th respectively and together with estimates of porosity and rock density (APLNG 2014; Smith 2015) result in an in situ production rate of $1 \cdot 10^{-11}$ cc(STP)/(g·year). The concentration of ^{4}He in solubility equilibrium is ca. $5 \cdot 10^{-8}$ cc(STP)/g and can be determined with an accuracy of better than 10%. The in situ produced helium component would therefore be distinguishable from solubility equilibrium earliest after 500-1000 years and then increase linearly with time. This makes helium a dating tracer that has no theoretical upper limit of application.

As outlined in Torgersen and Stute (2013) this linear increase is hardly ever fulfilled and influx of helium from aquitards and underlying formations as well as diffusive losses of helium from the aquifer to surrounding formations dominate the concentration behaviour with time. Therefore any interpretation of helium has to be treated at least with as much caution as for ^{14}C and all tracers have to be combined with each other to derive estimates of flow rates and direction.
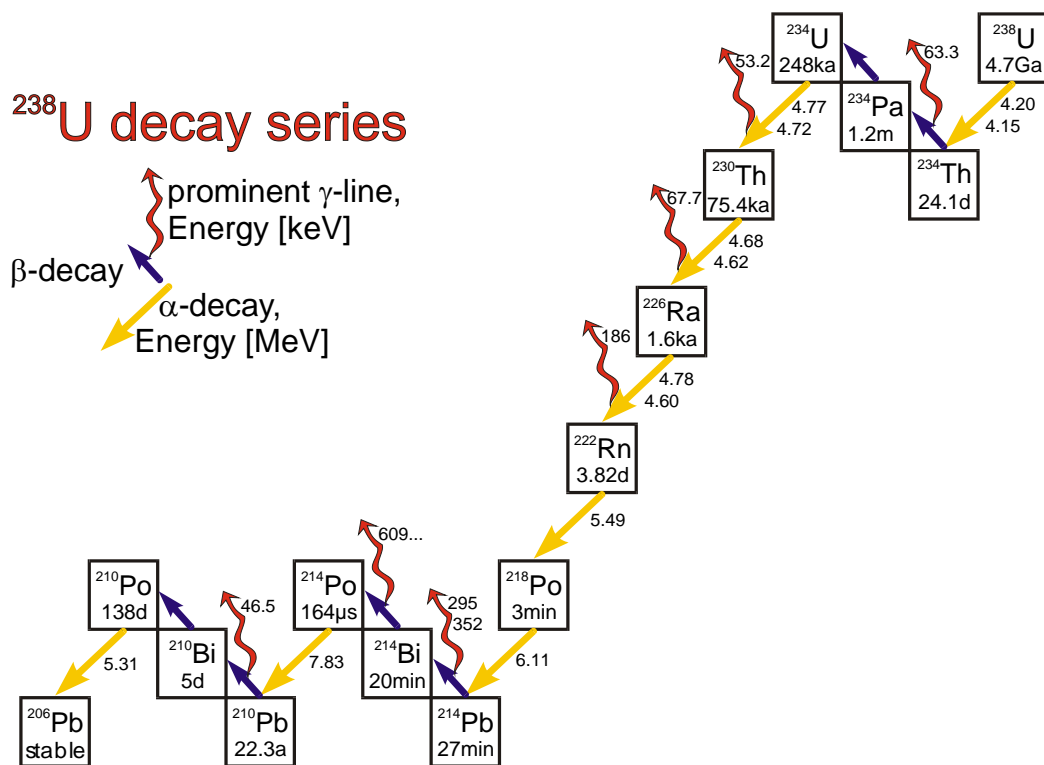

Figure A.3: Decay chain of ^{238}U (Suckow 2009), providing a total of 8 helium atoms per decaying ^{238}U (yellow arrows)

A.3   'Age' of groundwater is not a scalar but a distribution

Any groundwater sample contains not only one 'age', but many different ages (see Figure A.4 originating from (Torgersen *et al.* 2013)). The idea of an idealized age (as introduced in Section A.1) is displayed in Figure A.4 A. Wider age distributions are caused by diffusion and dispersion along a single flow path (Figure A.4 B). More realistically, flow paths from different parts of the recharge area start in the recharge area and meet in the well, causing a wider distribution than expected from diffusion and dispersion alone (Figure A.4 C). Furthermore, exchange with the aquitard matrix can strongly influence the age distribution (Figure A.4 D), which is discussed in more detail in the next paragraph. These processes together can create large discrepancies between apparent ages calculated for different tracers. This is due to the fact that each tracer 'sees' only a small part of the whole age distribution. Any calculation according to formulas like

Equation 3 therefore gives only an 'apparent age', and these apparent ages can differ easily by a factor of 2 or more for different tracers (Suckow 2013, 2014). The magnitude of the discrepancy between these apparent ages depends on the flow regime and on the sampling conditions.

However, all these processes A-D keep the age distribution in a uni-modal shape with only one maximum in the distribution. In reality this is even too simplistic an assumption. On long flow paths like several tens of kilometres, waters from different aquifers can mix, e.g. by the influence of faults or by windows in the aquitards separating the aquifers. This can cause bimodal or multimodal age distributions and render any apparent age meaningless (Figure A.4 E). Further downstream of such a confluence, hydrodynamic dispersion can then again spread out the difference between the single peaks and the age distribution can be uni-modal again, but much wider. This illustrates why the calculation of apparent ages in most cases is not a very useful approach (Suckow 2014) and is not followed in this report. Instead, different flow assumptions are tested against a multitude of tracers (Suckow 2013). Hereby it is necessary to always combine the tracers for 'old' groundwater (^{14}C, ^{4}He, ^{36}Cl) with those for young groundwater (CFCs, SF_6, ^{3}H) to de-convolute admixtures of young water in the sample (IAEA 2013).
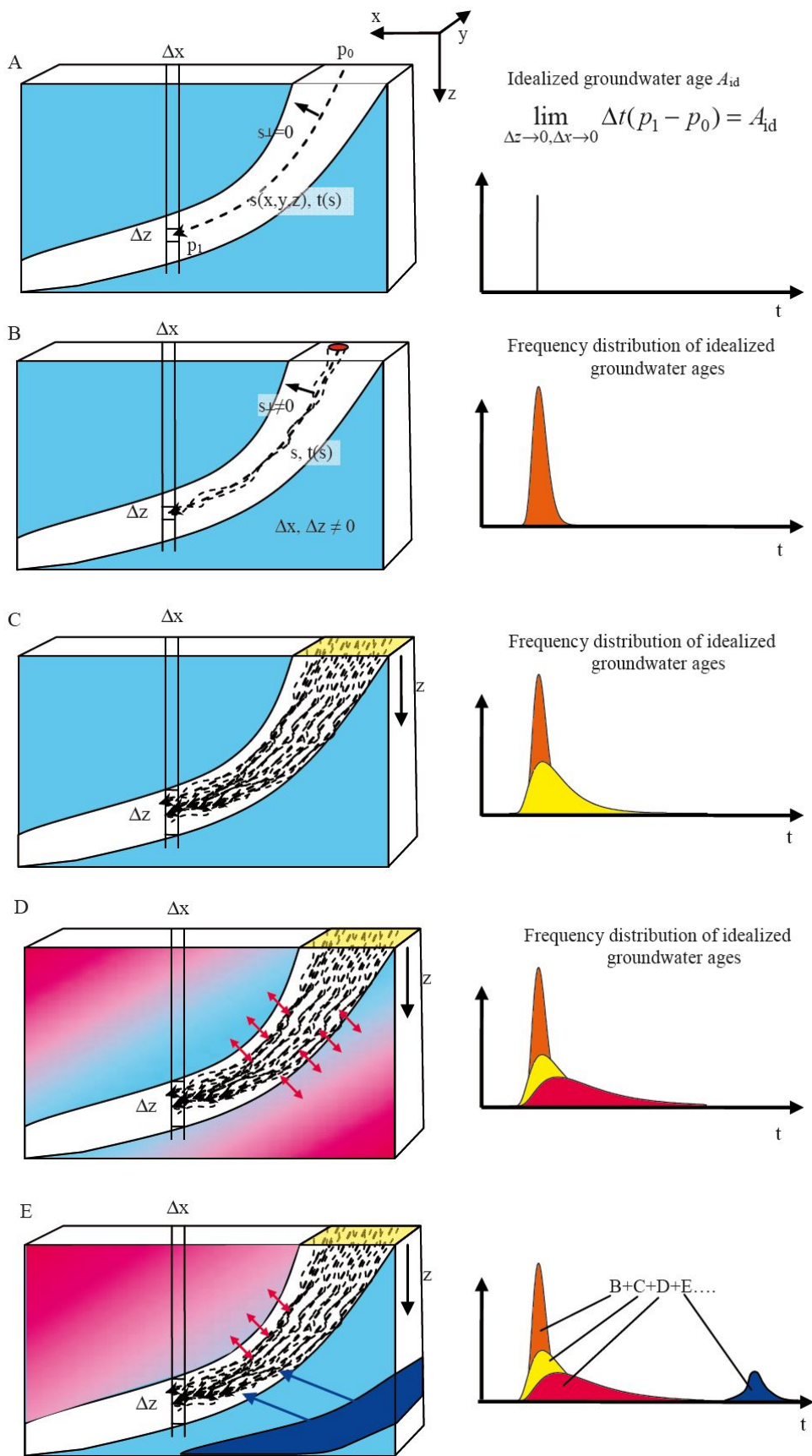
Figure A.4: Spreading of age distributions due to different processes relevant in groundwater (Torgersen et al. 2013)

A.4 Tracers in double porosity systems

Environmental tracers show special features in double porosity systems that may severely distort the derived flow velocity or apparent age. Double porosity here is defined as any situation in which the active flow system (the aquifer) can exchange any solutes (tracers) by diffusion with another stagnant part of the aquifer system. Such stagnant zones may exist in the aquifer itself (flow in fractures surrounding a stagnant matrix; preferential flow due to sedimentological differences), or these may be adjacent aquitards. In any case the flow in these zones is negligibly slow as compared to the aquifer. If the tracer concentration is lower in the stagnant zone as compared to the active flow zone, then the tracer is lost by diffusion into the stagnant zones. The length L is the distance how far the tracer can penetrate into the stagnant zone in a certain amount of time, and is only dependent on time t and the effective diffusion constant D' (Einstein 1905):

$$L(t) \cong \sqrt{D't} \qquad (7)$$

Variations of D' between different tracers in free water are up to a factor of 7 (e.g. at 10°C: $5.7 \cdot 10^{-9}$ m^2/s for ^{4}He (Jähne *et al.* 1987) and $0.8 \cdot 10^{-9}$ m^2/s for SF$_6$ (King and Saltzman 1995)). Diffusion rates decrease within the pore space of sediments due to tortuosity and this factor depends on details of the sediment properties but is normally also in the range of a factor of 10 or less. Furthermore, this tortuosity factor applies to all tracers the same way. Therefore the length $L(t)$ is mainly a function of time, and the differences in diffusion coefficients between tracers are of minor importance. If one assumes an aquifer of thickness a separated by stagnant layers (aquitards) of thickness b, then Figure A.5 illustrates the principle of tracer diffusion into the pore space (Purtschert *et al.* 2013).
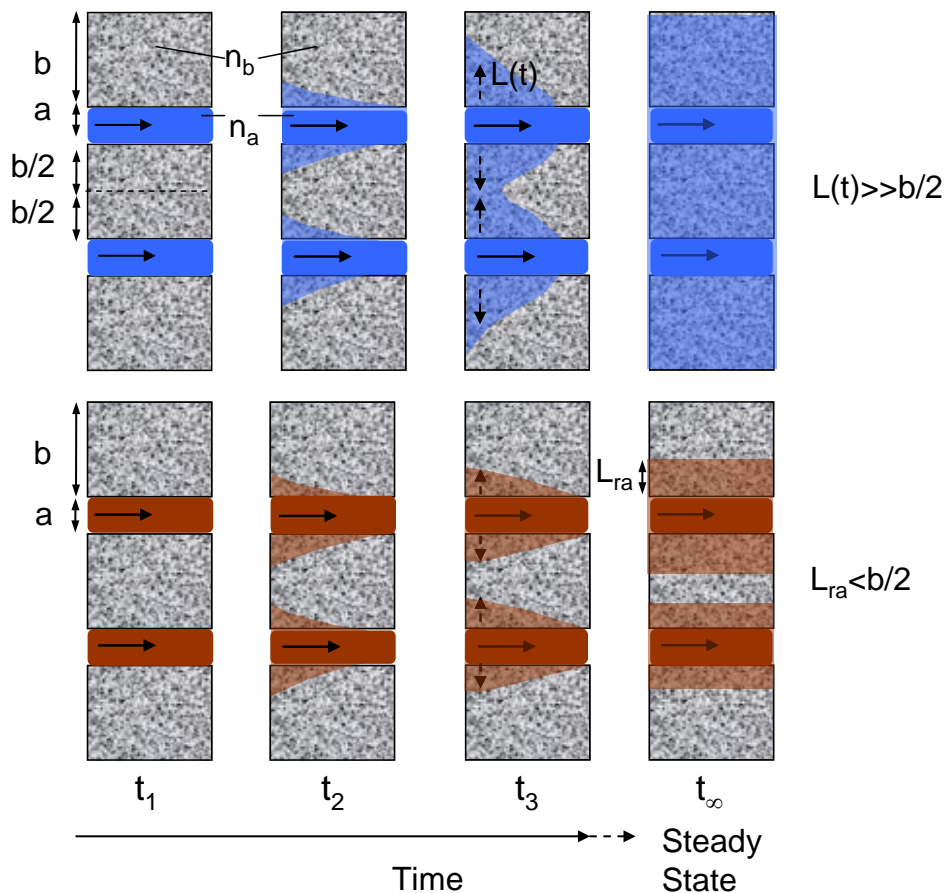

Figure A.5: Tracer retardation by matrix diffusive loss into stagnant zones (Purtschert *et al.* 2013)

Due to the diffusive loss into the aquitard, any environmental tracer that comes into the aquifer only with precipitation will result in a lower measured value if double porosity is important. This is true for ^{3}H, CFCs, SF$_6$, ^{14}C and [36]Cl and will result in a higher apparent age than the 'true' hydraulic age of the water. How much tracer is lost to the aquitard will depend on time (because $L(t)$ depends on time, see Equation 7 and the left part of Figure A.5) and for long times on the ratio of water volume in the stagnant zone to water volume in the aquifer (right part of Figure A.5). Also for a tracer produced in the underground, like [4]He, the groundwater will 'see' the much larger production volume of aquifer plus thickness $2 \cdot L(t)$ of the aquitard of which [4]He produced from uranium and thorium decay is released to the flowing groundwater. Again this will result in a higher apparent age than the 'true' hydraulic age of the water.

For a simple one-dimensional system of one thin aquifer in an extended aquitard that observes no flow but only molecular diffusion, Sudicky and Frind (1981) gave an analytic solution for the relationship of steady-state tracer concentration in the aquifer with distance:

$$C(x) = C_0 \cdot \exp\left(x \cdot \left(\frac{v}{2D} - \sqrt{\left(\frac{v}{2D}\right)^2 + \frac{\lambda}{D} + \frac{\sqrt{\lambda D'}}{D} \cdot \frac{n_b}{a \cdot n_a}} \right) \right) \tag{8}$$

Here c_0 is the initial tracer concentration at $x=0$, v is the flow velocity in the aquifer, λ the decay constant of the tracer, a the thickness of the aquifer and n_a and n_b are the porosities of aquifer and stagnant phases, respectively. D is the sum of hydrodynamic dispersion and diffusion in the aquifer, $D = \alpha_L \cdot v + D'$, where α_L is the dispersivity and D' the molecular diffusion of the tracer. The net effect of tracer loss by diffusion from the aquifer into the surrounding aquitard is that the radioactive tracer decreases (much) faster than according to radioactive decay. The effect can be easily a factor of ten or more, depending on aquifer thickness and travel distance. The resulting distribution of tracer versus distance is still exponential, as would be expected without the double-porosity effect. This makes it impossible to detect the importance of this effect from the tracer measurements alone if only *one* tracer is measured versus distance. Any apparent age as derived from a tracer like ^{14}C or [36]Cl would be larger than the flow time of water from the recharge to the sampling point.

This means, that the tracer loss manifests itself like a retardation factor R, in a similar manner as when chemical sorption occurs. This apparent retardation factor depends on the true hydraulic water age (represented as t), which in a steady state flow system is equivalent to flow distance x and on the ratio of available total volume to active flow volume (Maloszewski and Zuber 1985; Purtschert *et al.* 2013):

$$R(t) \cong \frac{a \cdot n_a + 2 \cdot L(t) \cdot n_b}{a \cdot n_a} \tag{9}$$

Here n_a and n_b are the porosities of the aquifer and the stagnant zones respectively. Obviously this retardation factor is time dependent; for very short times it is negligible ($L(t)=0$ in Equation 7, so $R=1$ at $t=0$) and increases with the square root of time. For a stable tracer the loss into the stagnant zones – and therefore the retardation factor – can be very large, because it can penetrate also into very thick stagnant zones. A radioactive tracer, however, may not have enough time to penetrate a thick stagnant zone b, because it decays earlier (lower part of Figure A.5). Therefore for a radioactive tracer the maximum length L_{ra} to which it can penetrate a stagnant layer, is dependent on the decay constant λ:

$$L_{ra} \cong \sqrt{\frac{D'}{\lambda}} \tag{10}$$

Obviously this maximum distance L_{ra} is the larger, the longer the half-life of the tracer is. Therefore in aquifer systems with very large stagnant layers like the Hutton Sandstone in the Surat Basin, also the *maximum* possible retardation factor increases with half live according to the following sequence:

$$R(t) \cong \frac{a \cdot n_a + 2 \cdot L_{ra} \cdot n_b}{a \cdot n_a}; \qquad R_{{}^3H} << R_{{}^{14}C} << R_{{}^{36}Cl} \tag{11}$$

One has to be aware that this sequence describes only the *maximum* retardation factor – after a flow distance x when the most short lived tracer (usually ^{3}H) reaches its L_{ra}, the retardation factors of the longer lived tracers (^{14}C and ^{36}Cl) will be nearly identical (distinguishable only due to the different diffusion constants in Equation 10), because for them $L(t)$ is still much smaller than L_{ra}. As a further consequence, this retardation factor is only constant at one point along the flow path in a system in steady state towards flow and transport. In any transient or stationary system, the retardation factor will increase along the flow path until either L_{ra} is reached or until tracer diffusion created a homogeneous concentration in aquifer and pore space (right state in Figure A.5). After this point in time and space no further net tracer loss from the aquifer will occur for a stable tracer, but still for a radioactive tracer.

The Sudicky model of Equation 8 fitted with two tracers for the same flow velocity allows deriving the total amount of water flowing within a deeper aquifer formation. This can be understood when re-arranging Equation 8 to the following form:

$$C(x) = C_0 \cdot \exp\left(\frac{x \cdot v}{2D} \left(1 - \sqrt{1 + \frac{4D}{v} \cdot \left(\frac{\lambda}{v} + \sqrt{\lambda D'} \cdot \frac{n_b}{a \cdot v \cdot n_a} \right)} \right) \right) \tag{12}$$

Here the terms in the exponential function have the following meaning: The term xv/D corresponds to the longitudinal Peclet number within the aquifer and describes how the tracer is spread within the aquifer in flow direction by dispersion. As mentioned earlier, dispersion is the product of dispersivity and flow velocity plus diffusion: $D = \alpha_L \cdot v + D'$. Since on the scales in discussion x is on the order of many 10,000 m and α_L is on the order of many meter, D' can be neglected and the term $xv/2D$ decomposes to $x/2\alpha_L$. The same holds true for the term $4D/v$ which decomposes to $4\alpha_L$. This allows for a Taylor development of the root in the exponential:

$$\sqrt{1 + x} \approx 1 + \frac{1}{2}x - \frac{1}{8}x^2 + \cdots \tag{13}$$

Which, together with the transformations of dispersion above allows us to transform the formula further:

$$C(x) \approx C_0 \cdot \exp\left(-x \cdot \frac{\lambda}{v} - x \cdot \sqrt{\lambda D'} \cdot \frac{n_b}{a \cdot v \cdot n_a} \right) \tag{14}$$

Note that this is independent of longitudinal dispersivity α_L, which explains the insensitivity of the Sudicky formula towards this parameter. As a result, in the case where the second porosity can be neglected ($n_b=0$) the whole exponential can be very well approximated by $\exp(-x\lambda/v)$ which corresponds to the transport of a radioactive tracer in a long tube. In cases where diffusion into the matrix is dominant for tracer loss, only the last term in the exponential becomes important. Here $\lambda D'$ is a measure of the length of matrix diffusion that is important for the tracer. This is largest for ^{36}Cl and is composed of physical constants and therefore not part of the fitting process and independent of the flow velocity or aquifer geometry. The term $n_b/(a \cdot v \cdot n_a)$ dominates the exponential decrease of tracer along the flow path and the fitting. The term $a \cdot v \cdot n_a$ is the amount of groundwater (in cubic meters per year) that is flowing through the aquifer in a vertical cross section per meter of aquifer length (thickness perpendicular to the cross section). Therefore, if diffusion into the matrix dominates the transport process, fitting of two independent tracer profiles like ^{14}C and ^{36}Cl to the Sudicky model gives an independent and comparably robust estimate of the amount of water flowing in the deeper parts of a thin confined aquifer.